Supplementary Information

Anti AIE single molecular fluorescent switch for detection of heavy metal ions

Yi-Mei Peng,[a] Yu-Ming Guan,[a] Qixia Bai,[a] Gang Chen,[a] Wei-Quan Lin,[b] Jing-Xian Pang,[a] Wen-Bo Xu,[a] Pingshan Wang,*[a] and Ting-Zheng Xie*[a]

Table of Contents

1. Synthetic route of ligand L

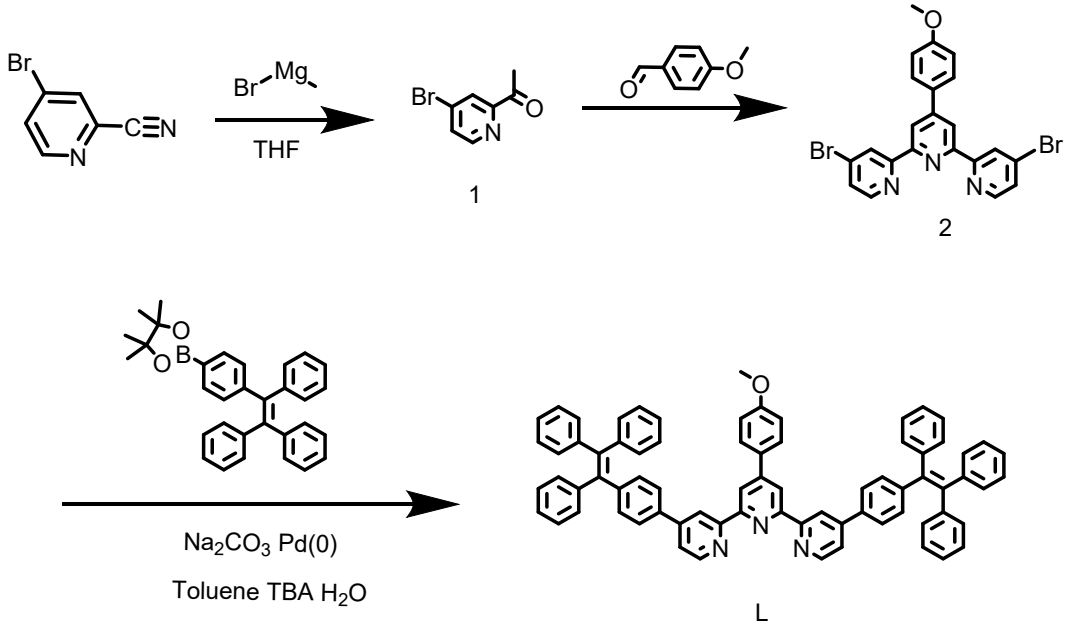

Scheme S1. Synthesis of ligand **L**

2. Experimental section

General procedures. Chemicals were purchased from Sigma/Aldrich, Energy Chemical, Bidepharm and used without further purification. Thin-layer chromatography (TLC) was conducted on flexible sheets (Baker-flex) precoated with Al_2O_3 (IB-F) or SiO_2 (IB2-F). Column chromatography was conducted using basic Al_2O_3 Brockman Activity I (60-325 mesh) or SiO_2 (60-200 mesh) from Fisher Scientific. NMR spectra were recorded on Bruker NMR 400 spectrometers, using $CDCl_3$ for ligand, CD_3CN for complexes. ESI mass spectrometry (MS) experiments were performed on a Waters Synapt HDMS G2-Si quadrupole/time-of-flight (Q/TOF) tandem mass spectrometer. This instrument contains a triwave device between the Q and TOF analyzers, consisting of three collision cells in the order trap cell, ion mobility cell, and transfer cell. Trap and transfer cells are pressurized with Ar, and the ion mobility cell is pressurized with N_2 flowing in a direction opposite to that of the entering ions.

Mass Spectrometry and Ion Mobility. ESI-MS and TWIM-MS were recorded with a Waters Synapt G2-Si tandem mass spectrometer, using solutions of 0.01 mg sample in 1 mL of $CHCl_3/CH_3OH$ (v/v, 1:3) for ligand or 0.5 mg sample in 1 mL of CH_3CN for complexes. All samples were infused into the ESI source at a flow rate of 6 μL/min by a syringe pump (KDS-100, KD Scientific). The TWIM-MS experiments were performed under the following conditions: ESI capillary voltage, 2 KV; sample cone voltage, 35 V; source offset, 42 V; source temperature 150 ℃; desolvation temperature, 250 ℃; cone gas flow, 10 L/h; desolvation gas flow, 700 L/h (N_2); source gas control, 0 mL/min; trap gas control, 3 mL/min; helium cell gas control, 120 mL/min; ion mobility (IM) cell gas control, 30 mL/min; sample flow rate, 8 μL/min; IM traveling wave height, 25 V; and IM traveling wave velocity, 1200 m/s. Data were collected and analyzed by using Mass Lynx 4.2 and Drift Scope 2.9.

Molecular Modeling. Energy minimization of the macrocycles was conducted with the Materials Studio version 6.0 program, using the Anneal and Geometry Optimization tasks in the Forcite module (Accelrys Software, Inc.). The counterions were omitted. Geometry optimization used a universal forcefield with atom-based

summation and cubic spline truncation for both the electrostatic and van der Waals parameters.

UV-Vis absorption and fluorescence properties. UV-Vis absorption spectra were recorded on a Thermo Fisher Scientific Evolution 201 spectrophotometer at room temperature in $CHCl_3/CH_3OH$ (v/v, 1:3) and were corrected with the background spectrum of the solvent. Fluorescence properties were performed on Edinburgh-FS5 Fluorescence spectrometer at 300 K in $CHCl_3/CH_3OH$ (v/v, 1:3).

Single crystal X-ray diffraction. Single crystal of **NAIE-Zn** suitable for X-ray diffraction was obtained by crystallization from CH_3CN/isopropyl ether solution (10 mg/mL) at 15 ℃. Single-crystal X-ray diffraction data for **NAIE-Zn** was collected on a Bruker D8 VENTURE diffractometer using a mirror monochromated Ga-Kα radiation. Using Olex2, the structures were solved with the SIR2004[2] structure solution program using Direct Methods and refined with the XH[3] refinement package using CGLS minimisation. Data refinement and reduction were undertaken with Bruker SAINT. The structures were solved by direct methods and refined by full-matrix least-squares on F2 with anisotropic displacement using the SHELXTL software package. Details on crystals data collection and refinement were summarized in Table **S1**. CCDC: 2414207.

3. Synthesis of the compounds and NAIE

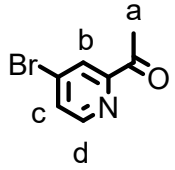

Compound 1: 4-methylpicolinonitrile (5 g, 42.3 mmol) and magnesium bromide (42 mL, 36.5 mmol) were added to a 250 mL round-bottomed flask, anhydrous and

oxygen-free tetrahydrofuran (20 mL) was added, and after stirring for 2 hours in an ice bath, the mixture was first burst with water to extinguish the magnesium bromide until there were no air bubbles, then 10 mL of 15% dilute hydrochloric acid was added, and finally the mixture was extracted with dichloride several times until the aqueous layer was clarified, to obtain the black oily compound **1** (4.5 g, 78.7%). ^{1}H NMR (500 MHz, $CDCl_3$) δ 8.49 (d, *J* = 5.0 Hz, 1H ,*Ph-H^d*), 8.19 (s, 1H, *Ph-H^b*), 7.63 (d, *J* = 5.0 Hz, 1H, *Ph-H^c*), 2.70 (s, 3H, *-CH$_3$-H^a*).

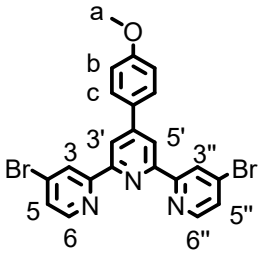

Compound 2: Compound **1** (4.2 g, 21.0 mmol), 4-methoxybenzaldehyde (1.43 g, 10.5 mmol), potassium hydroxide (1.18 g, 21.0 mmol) and ethanol (60 mL) were put into a three-necked flask, stirred at room temperature for 12 hours, then the temperature was raised to 65 ℃, NH_3·H_2O (55 mL, 3.0 mol) was added and stirred overnight, the reaction was stopped and then cooled, a solid was precipitated, filtered, and washed with deionized water for 3 times and then washed three times with isopropanol to obtain a white solid in a yield of 82%.^{1}H NMR (500 MHz, $CDCl_3$) δ 8.80 (d, *J* = 2.0 Hz, 2H, tpy-*H$^{3',5'}$*), 8.71 (s, 2H, tpy-*H$^{3,3''}$*), 8.53 (d, *J* = 5.0 Hz, 2H, tpy-*H$^{6,6''}$*), 7.85 (d, *J* = 9.0 Hz, 2H, *Ph-H^c*), 7.54 (dd, *J* = 5.0, 2.0 Hz, 2H, tpy-*H$^{5,5''}$*), 7.04 (d, *J* = 9.0 Hz, 2H, *Ph-H^b*), 3.89 (s, 3H, -CH_3-*H^a*).^{13}C NMR (101 MHz, $CDCl_3$) δ 160.73, 157.41, 154.70, 150.00, 149.82, 133.95, 130.28, 128.50, 127.06, 124.69, 119.17, 114.44, 55.42.

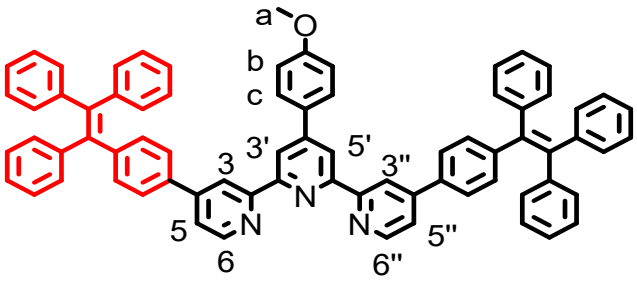

Ligand L: A 250 mL three-neck flask was charged with Compound 2 (100 mg, 0.201 mmol), 4,4,5,5-tetramethyl-2-(4-(1,2,2-triphenylvinyl)phenyl)-1,3,2-dioxaborolane (230 mg, 0.503 mmol), $Pd(PPh_3)_4$ (20 mg, 0.017 mmol) and sodium carbonate (142 mg, 1.344 mmol). 25 ml of toluene, 15 ml of H_2O and 10 ml of tert-butanol were added under N_2. The mixture was stirred at 85 ℃ for 2 days. After cooling to room temperature, the mixture was extracted with CH_2Cl_2. The combined organic layers were washed with brine, dried over anhydrous Na_2SO_4, and concentrated in vacuo. The residue was purified by dry column chromatography (SiO_2), eluting with DCM/MeOH (100:1, v/v) to give 150 mg of white solid product (75% yield).^{1}H NMR (500 MHz, $CDCl_3$) δ 8.85 (s, 2H, tpy-*H$^{3',5'}$*), 8.73 (d, *J* = 5.0 Hz, 2H, tpy-*H$^{3,3''}$*), 8.70 (s, 2H,

tpy-$H^{6,6''}$), 7.90 (d, *J* = 6.0 Hz, 2H, tpy-$H^{5,5''}$), 7.56 (d, *J* = 13.0 Hz, 6H, *Ph*-$H^{b,c,h}$), 7.21 – 6.95 (m, 36H, *Ph*-H^{h}), 3.90 (s, 3H, -CH_3-H^{a}).^{13}C NMR (101 MHz, $CDCl_3$) δ 160.57, 156.91, 155.99, 149.82, 149.59, 148.58, 144.97, 143.53, 143.45, 143.38, 141.84, 140.20, 136.09, 132.11, 131.37, 131.34, 131.30, 130.75, 128.58, 127.90, 127.83, 127.73, 126.73, 126.69, 126.61, 126.31, 121.28, 119.15, 118.59, 114.37, 55.41.

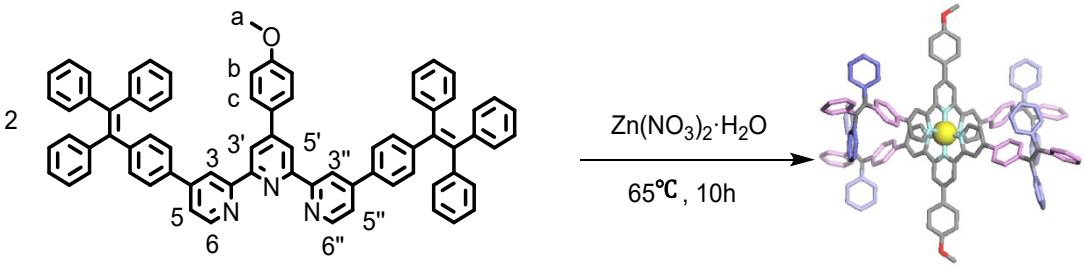

NAIE (**ZnL_2**): To a solution of ligand **L** (10.0 mg, 10.0 mmol) in $CHCl_3$ (8 mL) was added a solution of $Zn(NO_3)_2$•$6H_2O$ (1.49 mg, 5.0 mmol) in MeOH (10 mL). The mixture was stirred at 60 ℃ for 8 h and cooled to room temperature, then an excess of NH_4PF_6 was added for anion exchange, and the precipitate was washed with water and then methanol, and dried under vacuum to give a yellow solid (16.0 mg, 77.8%).^{1}H NMR (500 MHz, CD_3CN) δ 9.06 (s, 4H, tpy-$H^{A3',5'}$), 8.85 (s, 4H, tpy-$H^{A3,3''}$), 8.25 (d, *J* = 7.0 Hz, 4H, tpy-$H^{A5,5''}$), 7.79 (s, 4H, tpy-$H^{A6,6''}$), 7.66 (d, *J* = 7.0 Hz, 8H, *Ph*-H^{c}), 7.55 (s, 4H, *Ph*-H^{b}), 7.28 (s, 4H, *Ph*-H^{h}), 7.22 (d, *J* = 8.0 Hz, 8H,*Ph*-H^{h}), 7.09 (d, *J* = 43.0 Hz, 60H, *Ph*-H^{h}), 3.97 (s, 6H, -CH_3-H^{a}).ESI-TOF (*m/z*):2049.09 [M−2PF_6^-]$^{2+}$ (calcd *m/z*: 2049.09).

4. ESI-MS spectra data of NAIE (PF_6^- as counterion)

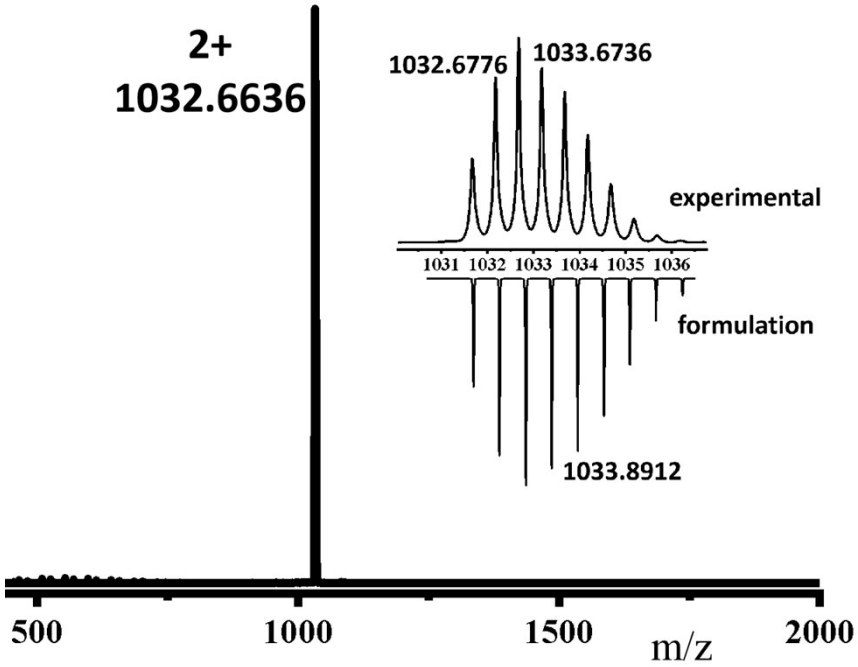

Figure S1. ESI-MS spectrum of **NAIE-Zn** (PF_6^- as counterion) with measured (top) and calculated (bottom) isotope patterns.

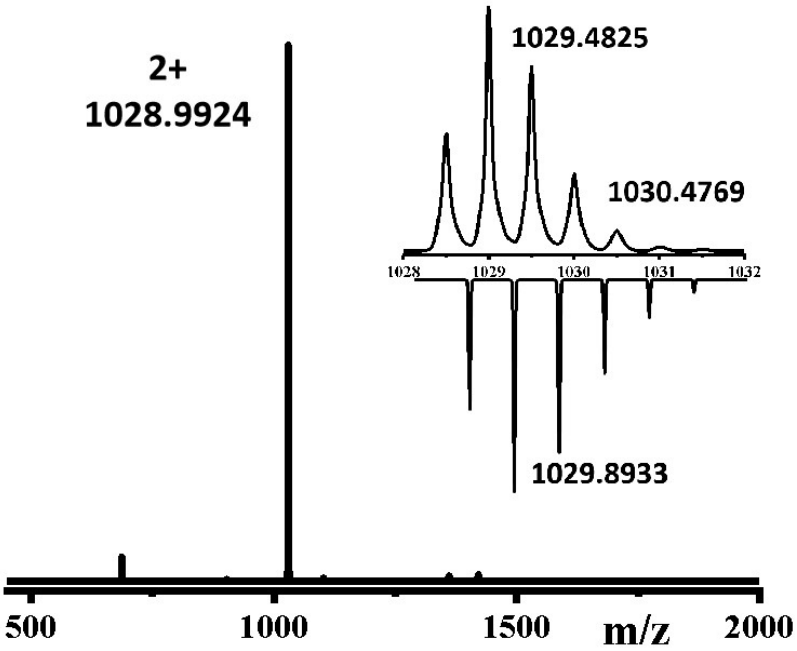

Figure S2. ESI-MS spectrum of **NAIE-Co** (PF_6^- as counterion) with measured (top) and calculated (bottom) isotope patterns.

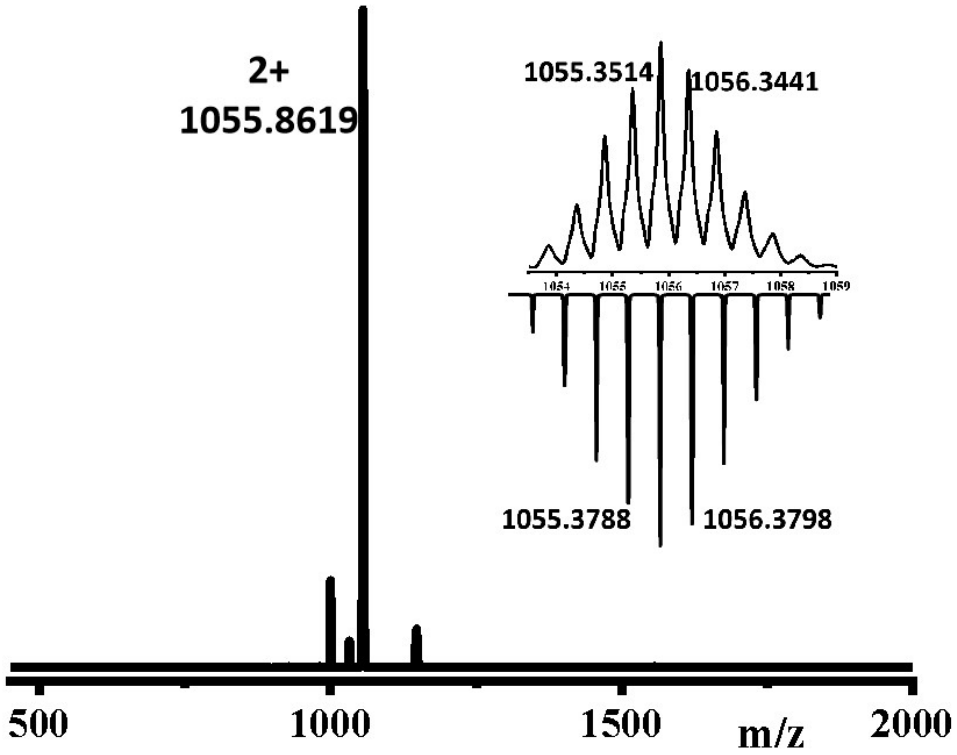

Figure S3. ESI-MS spectrum of **NAIE-Cd** (PF_6^- as counterion) with measured (top) and calculated (bottom) isotope patterns.

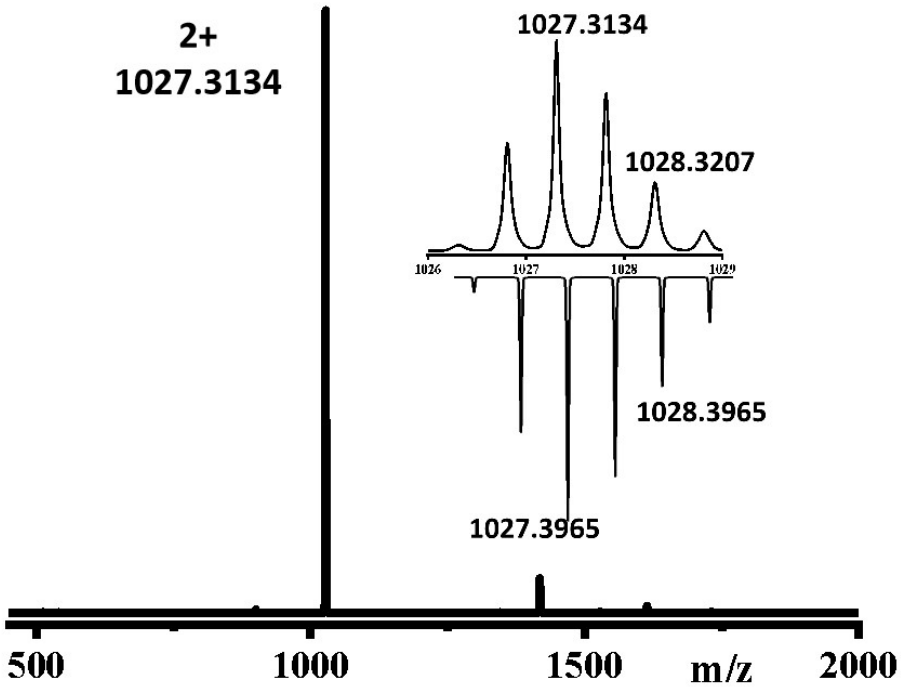

Figure S4. ESI-MS spectrum of **NAIE-Fe** (PF_6^- as counterion) with measured (top) and calculated (bottom) isotope patterns.

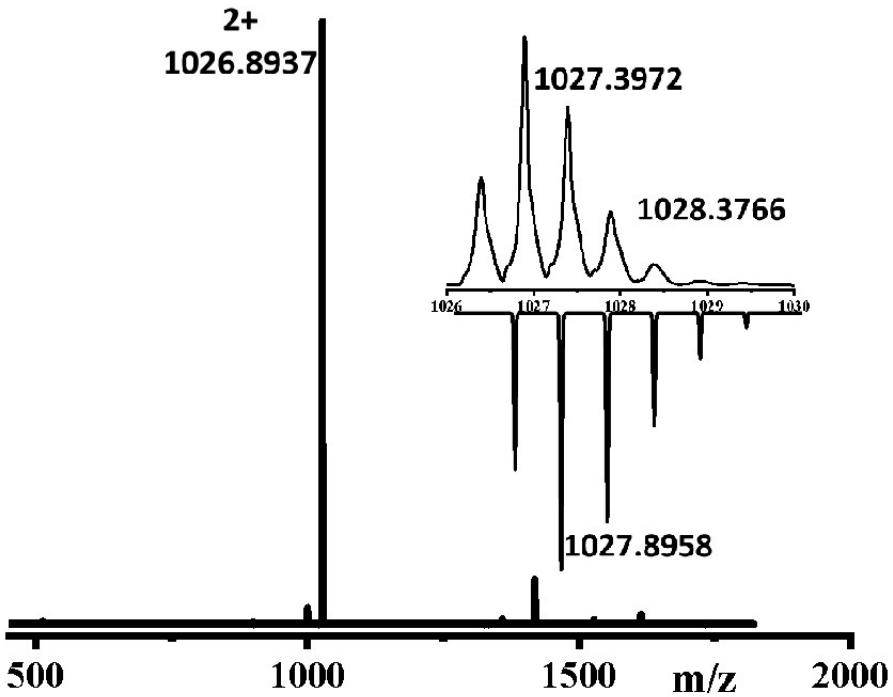

Figure S5. ESI-MS spectrum of **NAIE-Mn** (PF_6^- as counterion) with measured (top) and calculated (bottom) isotope patterns.

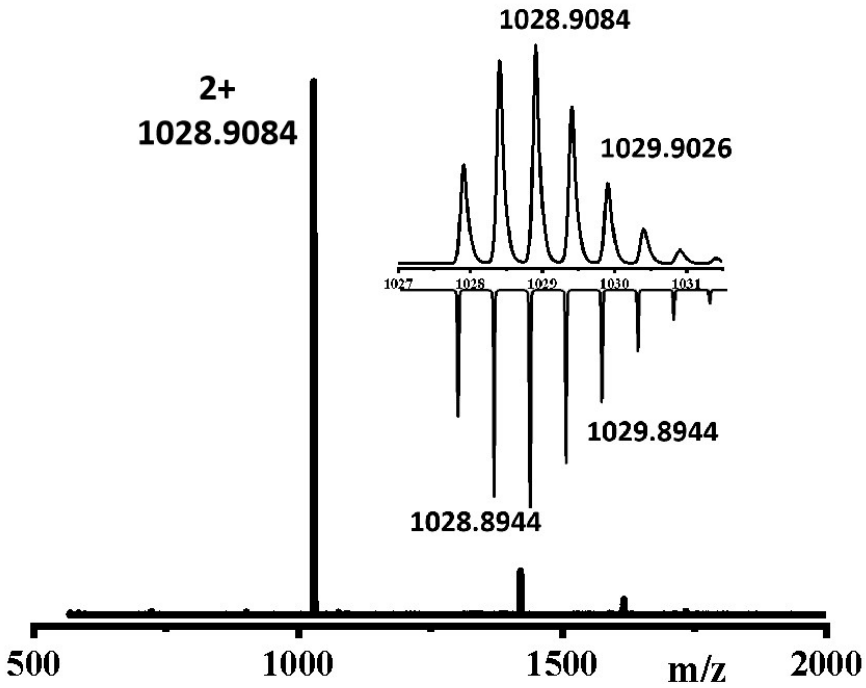

Figure S6. ESI-MS spectrum of **NAIE-Ni** (PF_6^- as counterion) with measured (top) and calculated (bottom) isotope patterns.

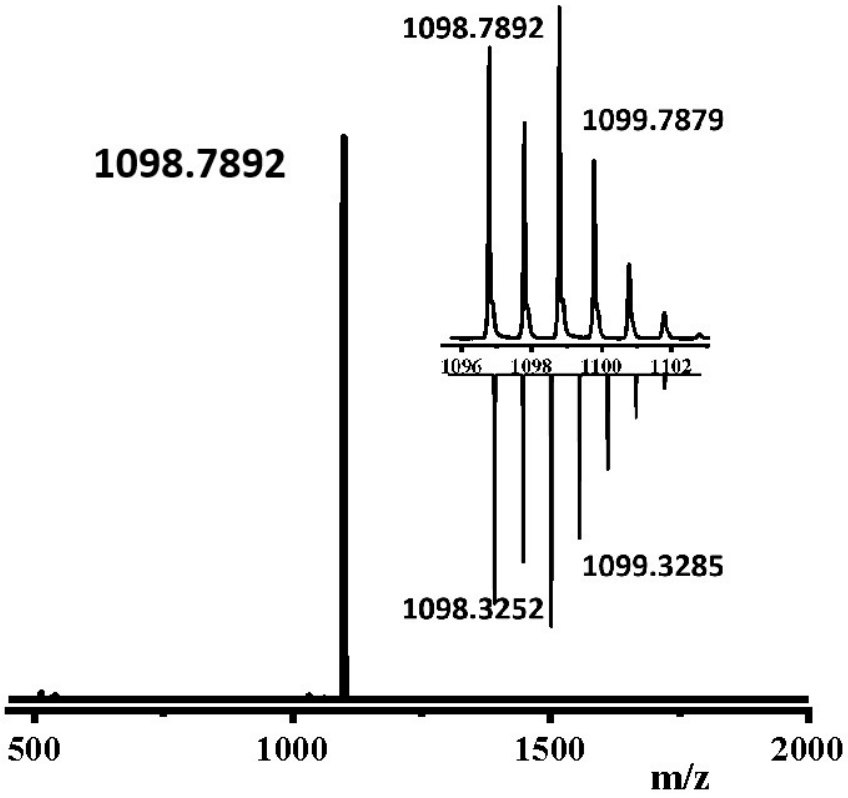

Figure S7. ESI-MS spectrum of **NAIE-Cu** (PF_6^- as counterion) with measured (top) and calculated (bottom) isotope patterns.

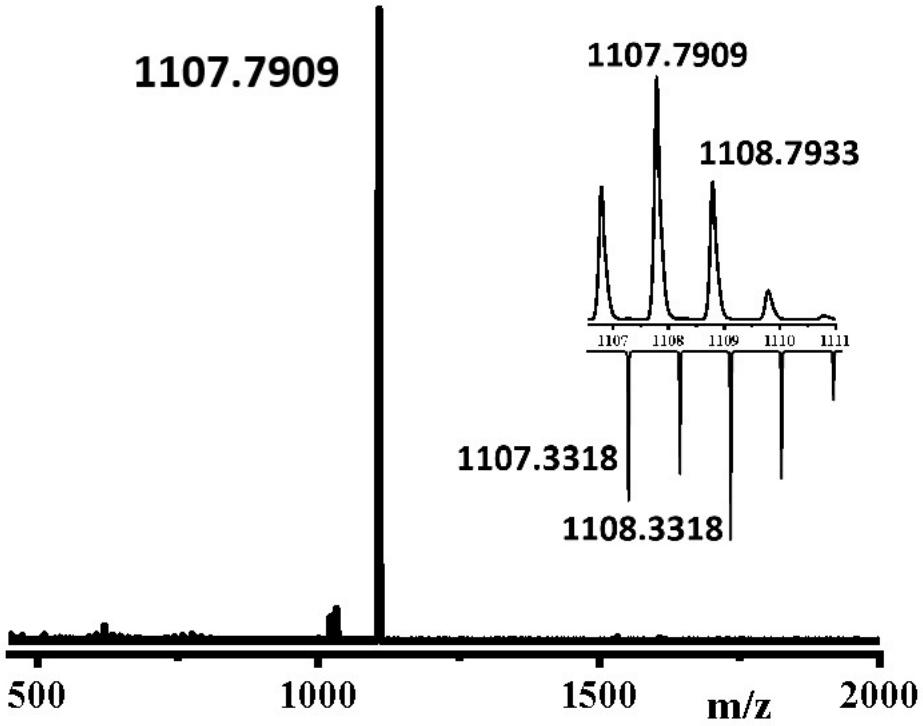

Figure S8. ESI-MS spectrum of **NAIE-Ag** (PF_6^- as counterion) with measured (top) and calculated (bottom) isotope patterns.

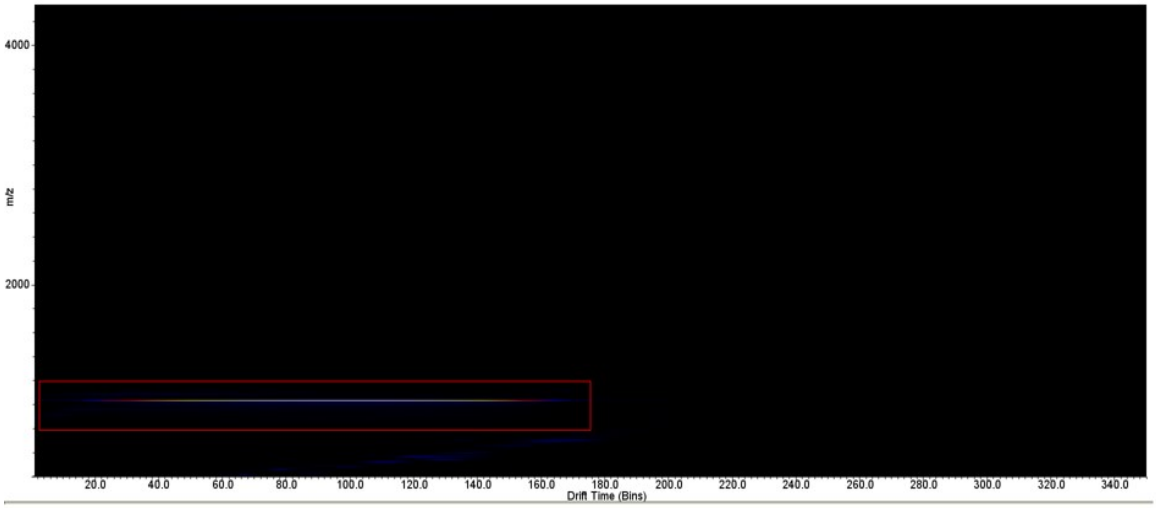

Figure S9. Two dimensional mass spectrum (TWIM-MS) of **NAIE Zn**(PF_6^- as counterion).

5. 1H, 13C, COSY, NOESY, NMR spectrum

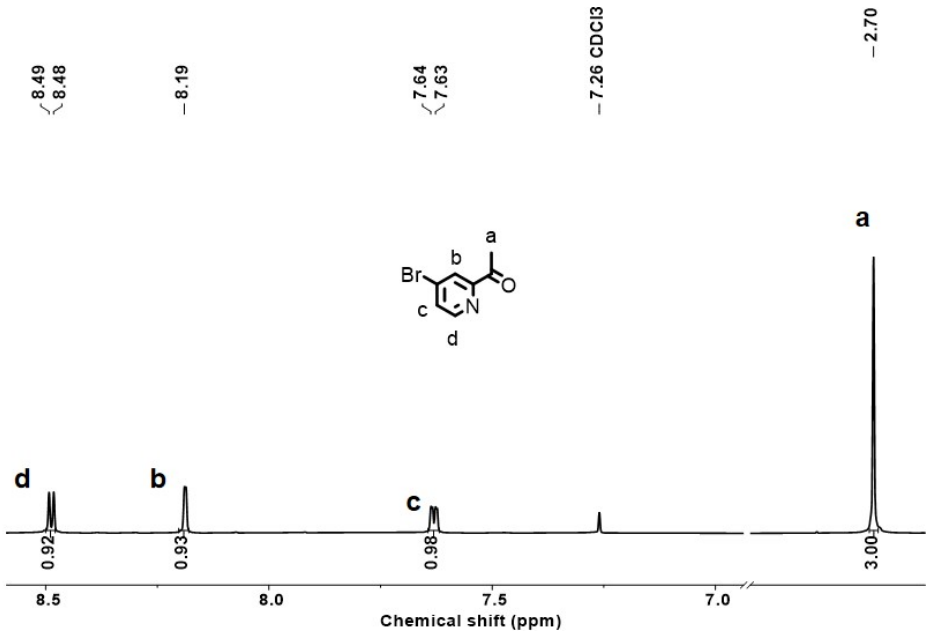

Figure S10. ^{1}H NMR (400 MHz, $CDCl_3$, 300 K) spectrum of compound **1**.

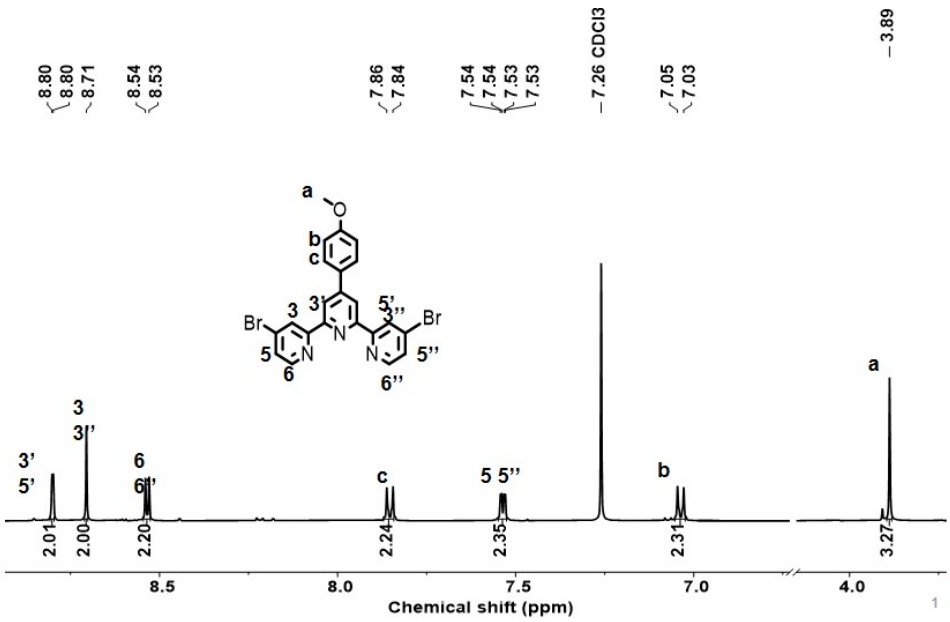

Figure S11. ^{1}H NMR (400 MHz, $CDCl_3$, 300 K) spectrum of compound **2**.

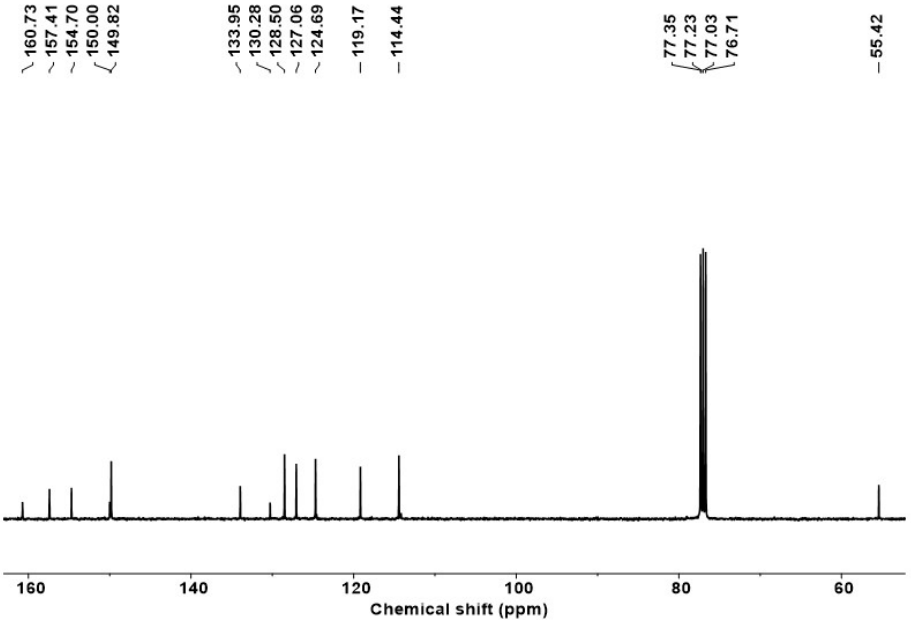

Figure S12. ^{13}C NMR (101 MHz, $CDCl_3$, 300 K) spectrum of compound **2**.

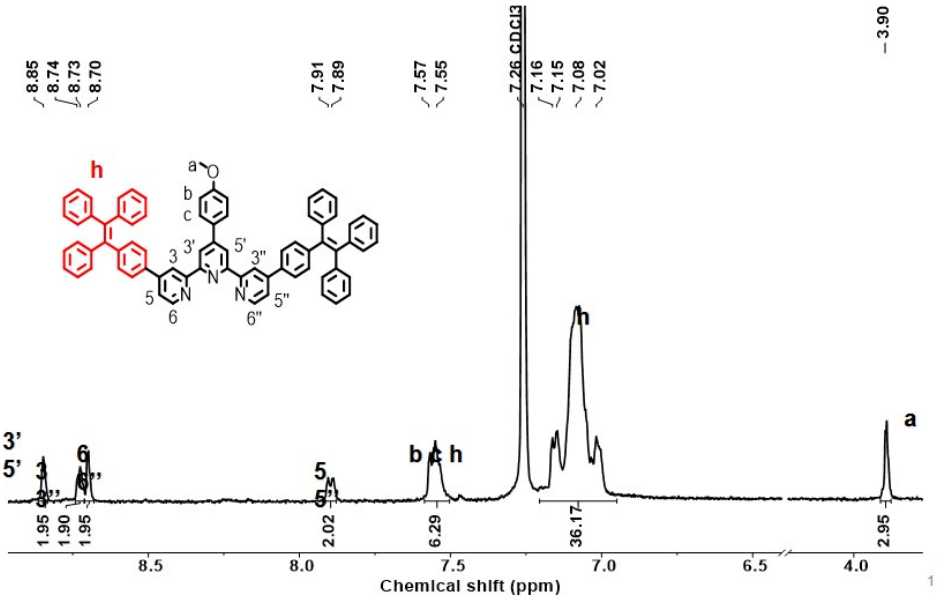

Figure S13. ^{1}H NMR (400 MHz, $CDCl_3$, 300 K) spectrum of Ligand **L**.

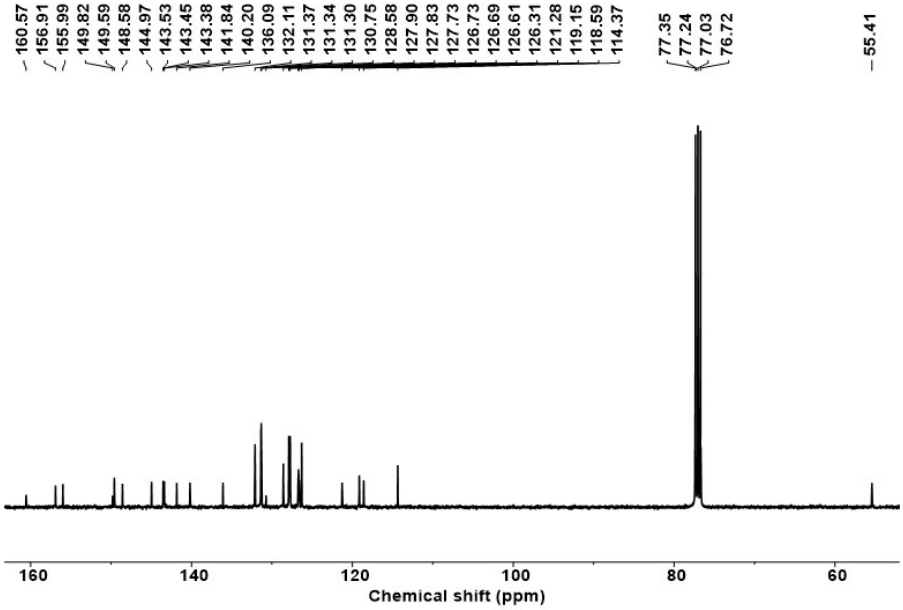

Figure S14. ^{13}C NMR (101 MHz, $CDCl_3$, 300 K) spectrum of Ligand **L**.

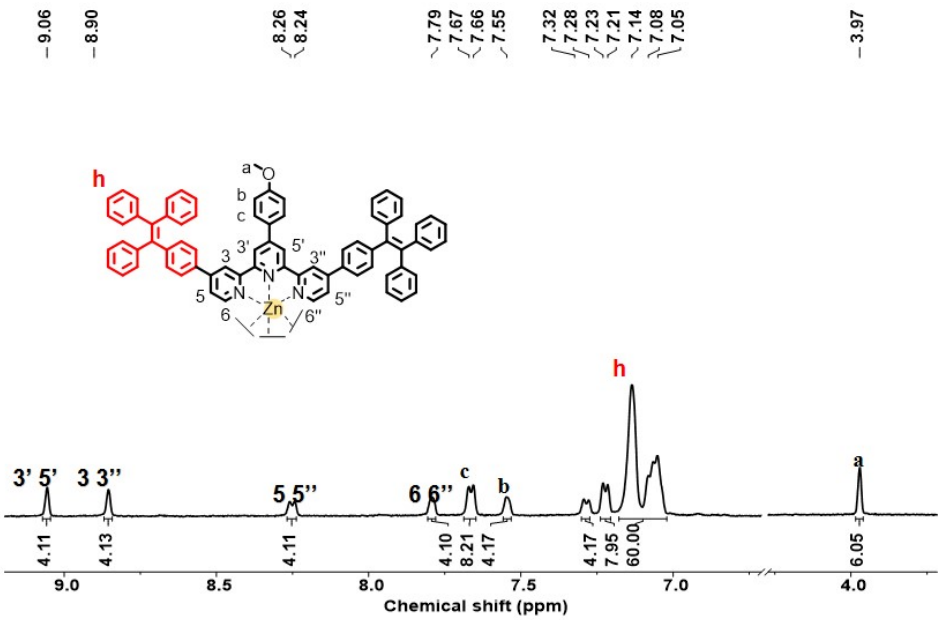

Figure S15. ^{1}H NMR (400 MHz, CD_3CN, 300 K) spectrum of **NAIE-Zn** .

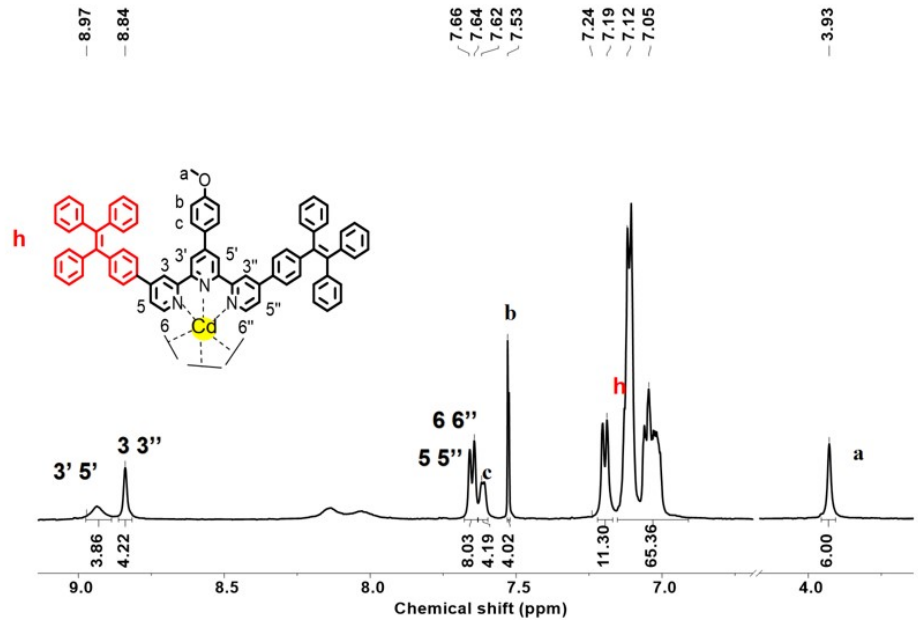

Figure S16. ^{1}H NMR (400 MHz, CD_3CN, 300 K) spectrum of **NAIE-Cd** .

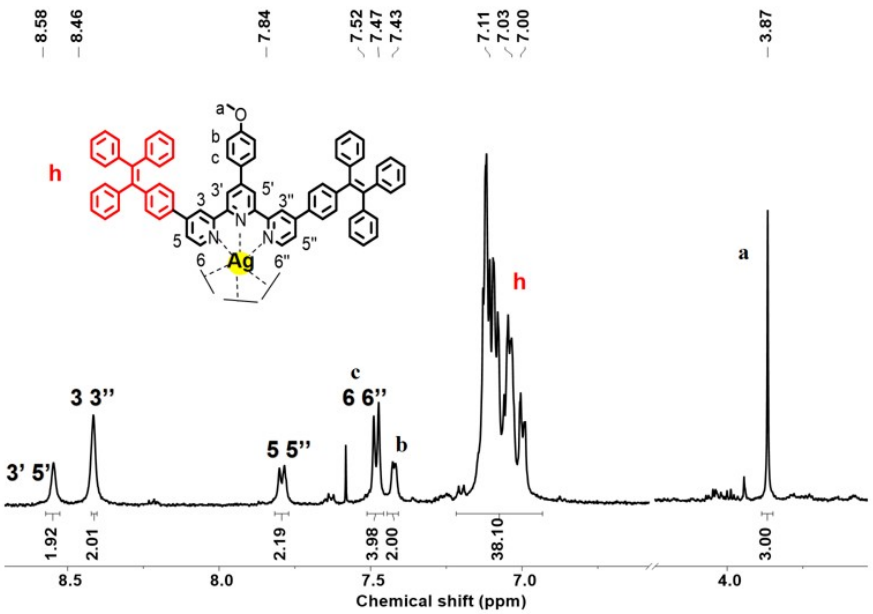

Figure S17. ^{1}H NMR (400 MHz, CD_3CN, 300 K) spectrum of **NAIE-Ag**.

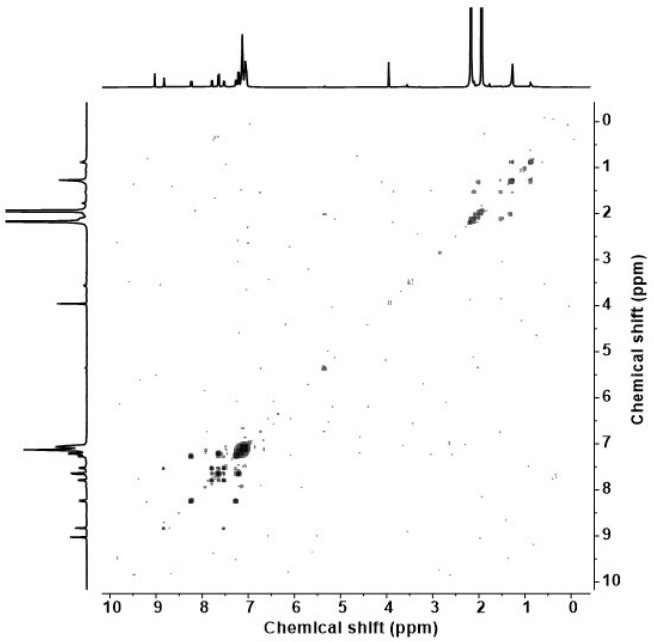

Figure S18. 2D COSY NMR (500 MHz, CD_3CN, 300 K) spectrum of **NAIE-Zn** (full spectrum).

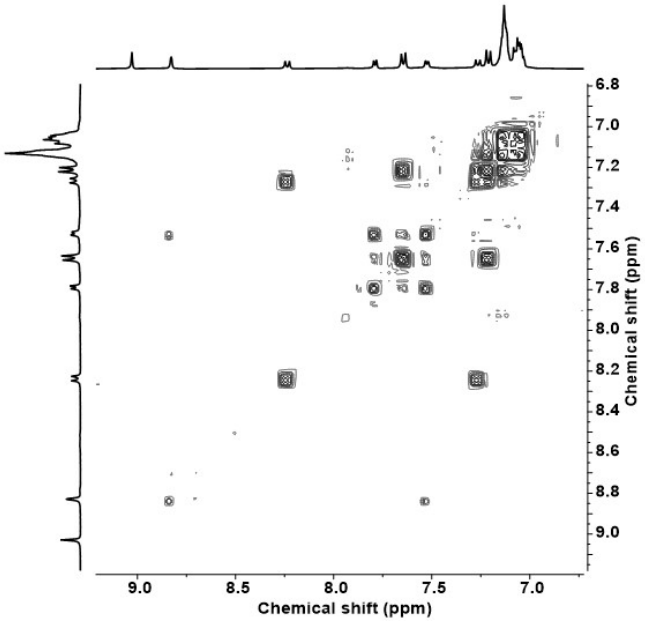

Figure S19. 2D COSY NMR (500 MHz, CD_3CN, 300 K) spectrum of **NAIE-Zn** (aromatic region).

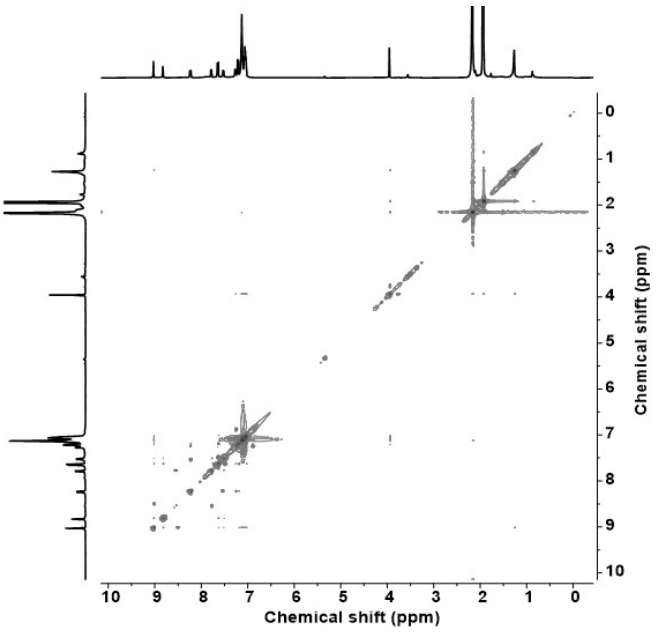

Figure S20. 2D NOESY NMR (500 MHz, CD_3CN, 300 K) spectrum of **NAIE-Zn** (full spectrum).

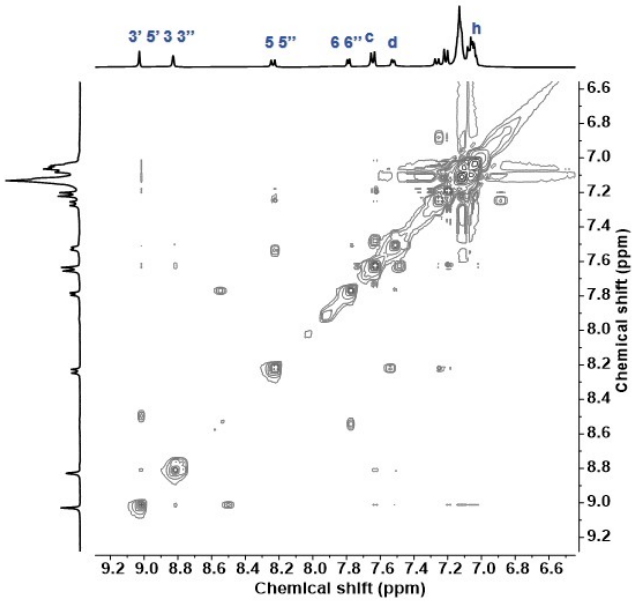

Figure S21. 2D NOESY NMR (500 MHz, CD_3CN, 300 K) spectrum of **NAIE-Zn** (aromatic region).

6. X-ray crystallographic data and structures

Table S1. Crystal Data and Structure Refinement for **NAIE-Zn**.

Identification code	**NAIE**
Empirical formula	$C_{148}H_{106}F_{12}N_6O_2P_2Zn$
Formula weight	2421.16
Temperature/K	100.0
Crystal system	monoclinic
Space group	C2/c
a/Å	56.299(3)
b/Å	9.2556(5)
c/Å	25.7870(14)
α/°	90
β/°	108.105(3)
γ/°	90
Volume/Å^3	12771.9(12)
Z	4
ρ_{calc}g/cm^3	1.259
μ/mm^{-1}	0.748
F(000)	4801.0

Crystal size/mm^3	0.13 mm× 0.1 mm× 0.08 mm
Radiation	GaKα (λ = 1.34139)
2Θ range for data collection/°	5.748 to 110.33
Index ranges	-66≤h≤68, -11≤k≤11, -31≤l≤31
Reflections collected	105310
Independent reflections	12203 [R_{int} = 0.0967, R_{sigma} = 0.0929]
Data/restraints/parameters	12203/0/803
Goodness-of-fit on F^2	1.530
Final R indexes [I>=2σ (I)]	R_1 = 0.1191, wR_2 = 0.3639
Final R indexes [all data]	R1 = 0.1501, wR2 = 0.3942
Largest diff. peak/hole / e Å^{-3}	1.72/-1.08

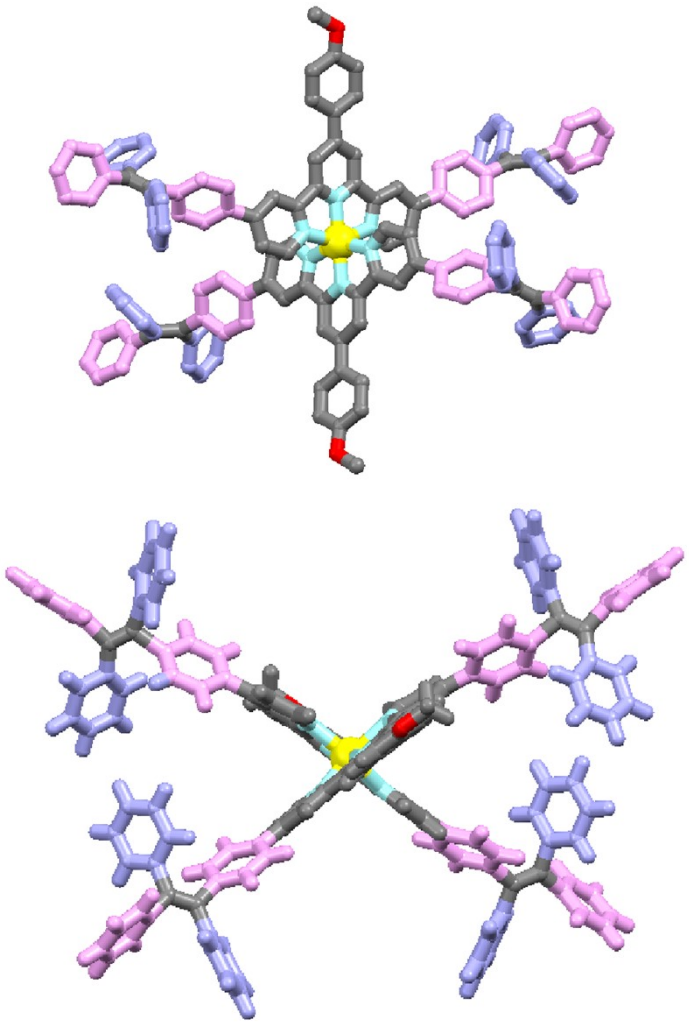

Figure S22. The calculation of **NAIE-Zn** in the monomer state showed a planar conformation.

7. Standards for drinking water quality

Table S2. Conventional water quality indicators and limits of metal ions($CHCl_3/CH_3OH$ (v/v, 1:3))

Indicators	Limits (mg/L)	limits of detection (mg/L)
Zn/(mg/L)	1.0	0.0016
Co/(mg/L)	1.0	0.0013
Cd/(mg/L)	0.005	0.00144
Cu/(mg/L)	1.0	0.000706
Fe/(mg/L)	0.3	0.001057
Ag/(mg/L)	0.05	0.001052
Mn/(mg/L)	0.1	0.00092
Ni/(mg/L)	0.02	0.002129
Pt/(mg/L)	0.01	0.0015
Ce/(mg/L)	/	0.001333
Eu/(mg/L)	0.001	0.00152
Zr/(mg/L)	/	0.001485

Table S3. Conventional water quality indicators and limits of metal ions（water system）

Indicators	Limits (mg/L)	limits of detection (mg/L)
Zn/(mg/L)	1.0	0.0140
Co/(mg/L)	1.0	0.0040
Cd/(mg/L)	0.005	0.0043
Cu/(mg/L)	1.0	0.0036
Fe/(mg/L)	0.3	0.0049
Ag/(mg/L)	0.05	0.0039
Mn/(mg/L)	0.1	0.0041
Ni/(mg/L)	0.02	0.0119
Pt/(mg/L)	0.01	0.0068
Ce/(mg/L)	/	0.0058
Eu/(mg/L)	0.001	0.0132

Zr/(mg/L)	/	0.0097

8. UV-vis and Fluorescence emission spectra of L and NAIE.

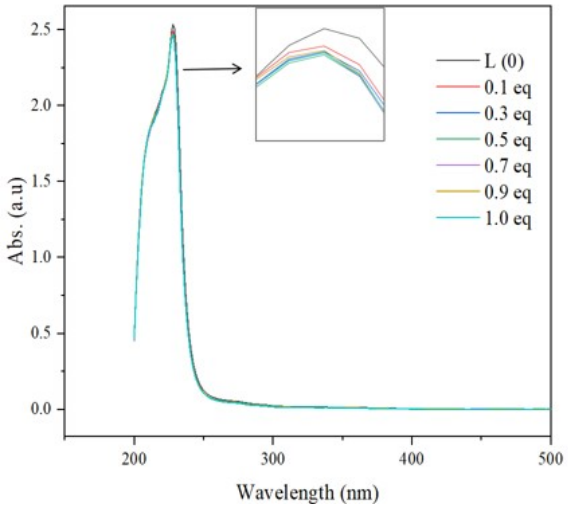

Figure S23. UV/vis absorption of **NAIE** in $CHCl_3/CH_3OH$ (v/v, 1:3) with different concentrations at 298 K.(Quartz fluorescence cell of 1 mm thickness were used for fluorescence and UV fluorescence testing)

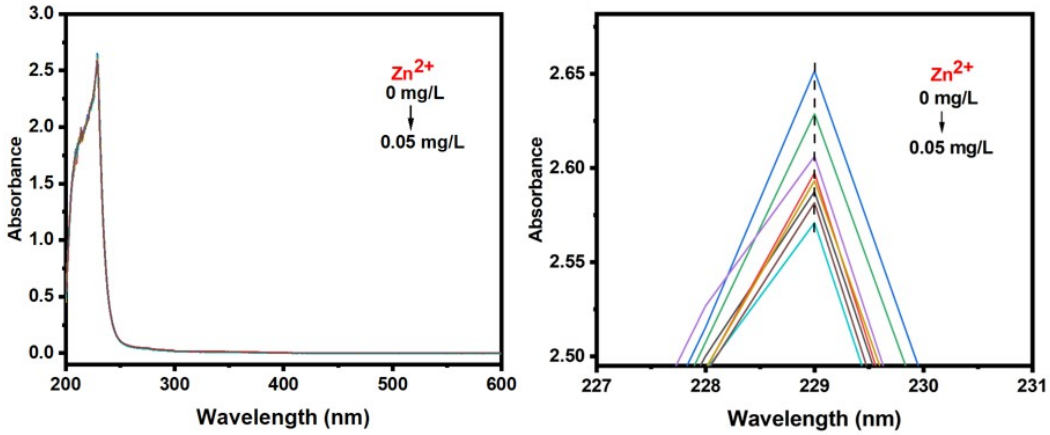

Figure S24. UV/vis absorption of **NAIE-Zn** in $CHCl_3/CH_3OH$ (v/v, 1:3) with different concentrations at 298 K.

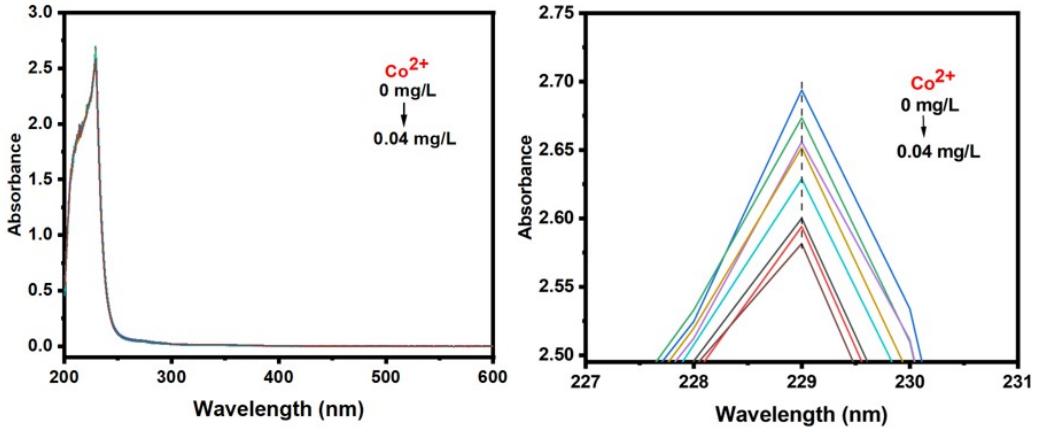

Figure S25. UV/vis absorption of **NAIE-Co** in $CHCl_3/CH_3OH$ (v/v, 1:3) with different concentrations at 298 K.

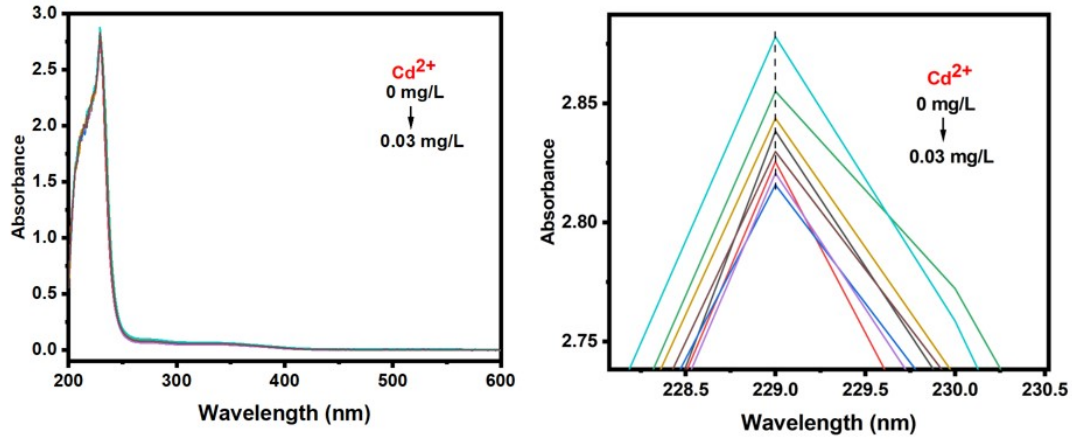

Figure S26. UV/vis absorption of **NAIE-Cd** in $CHCl_3/CH_3OH$ (v/v, 1:3) with different concentrations at 298 K.

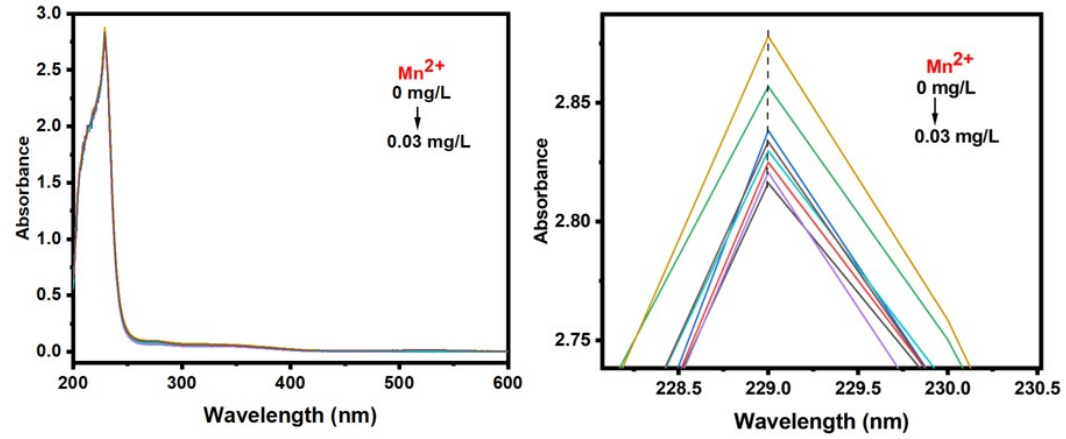

Figure S27. UV/vis absorption of **NAIE-Mn** in $CHCl_3/CH_3OH$ (v/v, 1:3) with different concentrations

at 298 K.

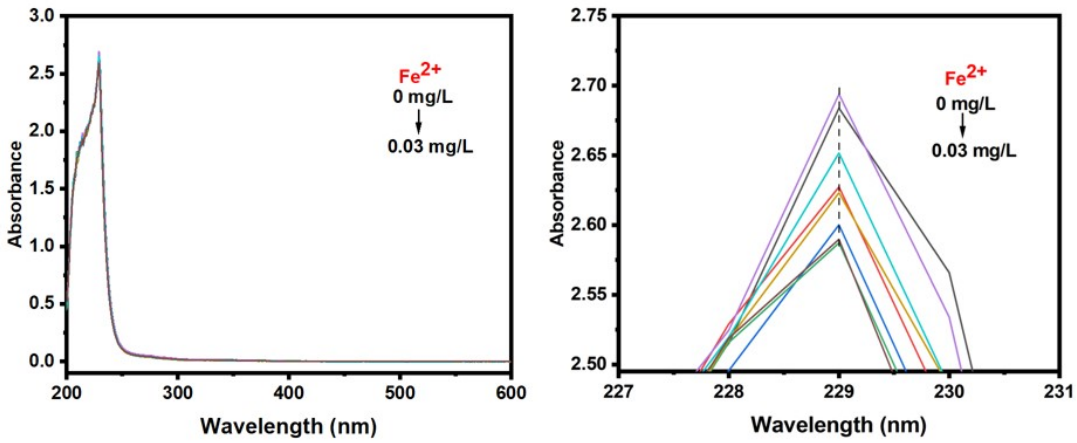

Figure S28. UV/vis absorption of **NAIE-Fe** in $CHCl_3/CH_3OH$ (v/v, 1:3) with different concentrations at 298 K.

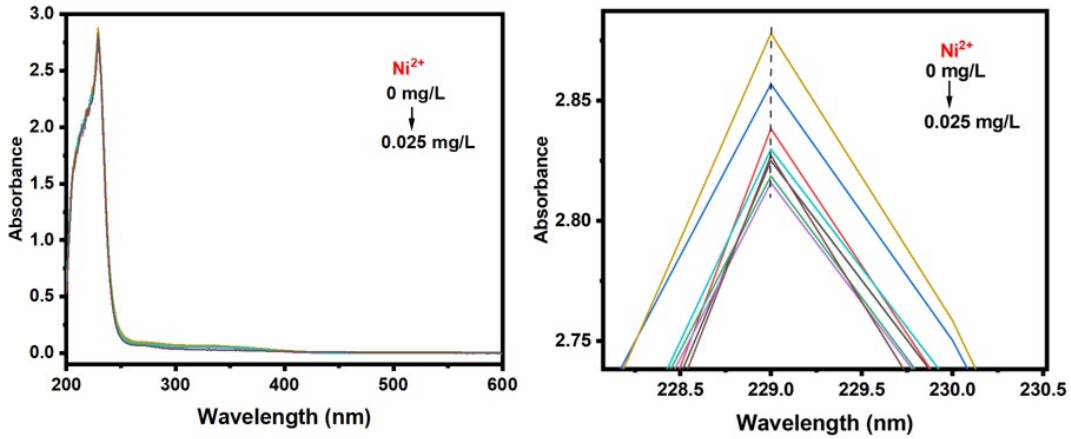

Figure S29. UV/vis absorption of **NAIE-Ni** in $CHCl_3/CH_3OH$ (v/v, 1:3) with different concentrations at 298 K.

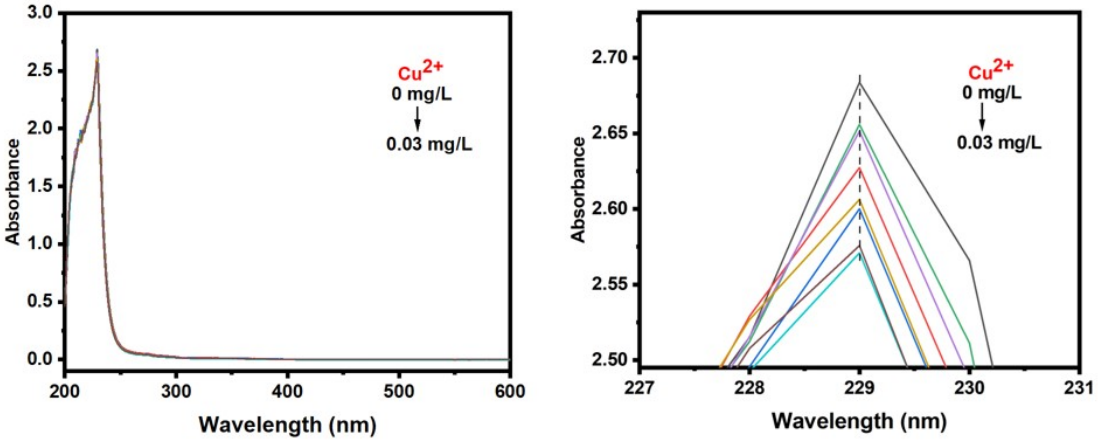

Figure S30. UV/vis absorption of **NAIE-Cu** in $CHCl_3/CH_3OH$ (v/v, 1:3) with different concentrations

at 298 K.

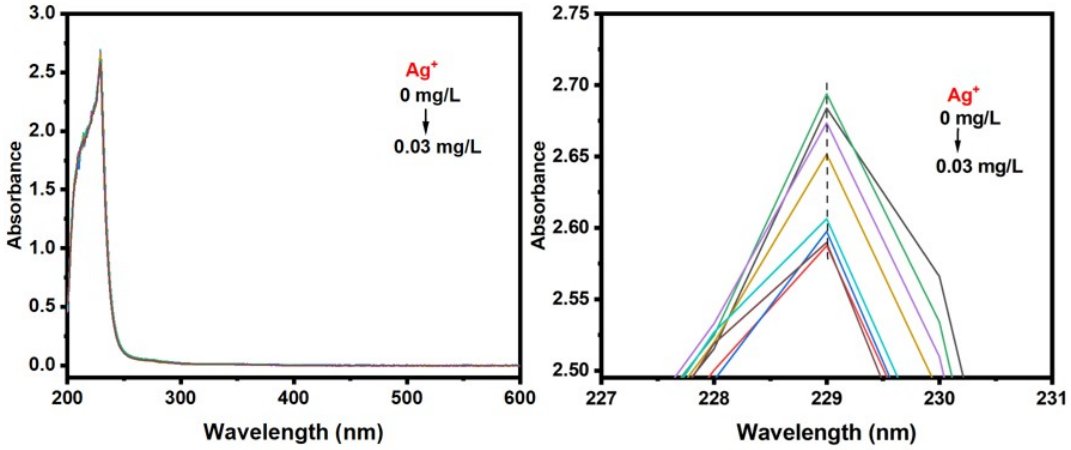

Figure S31. UV/vis absorption of **NAIE-Ag** in $CHCl_3/CH_3OH$ (v/v, 1:3) with different concentrations at 298 K.

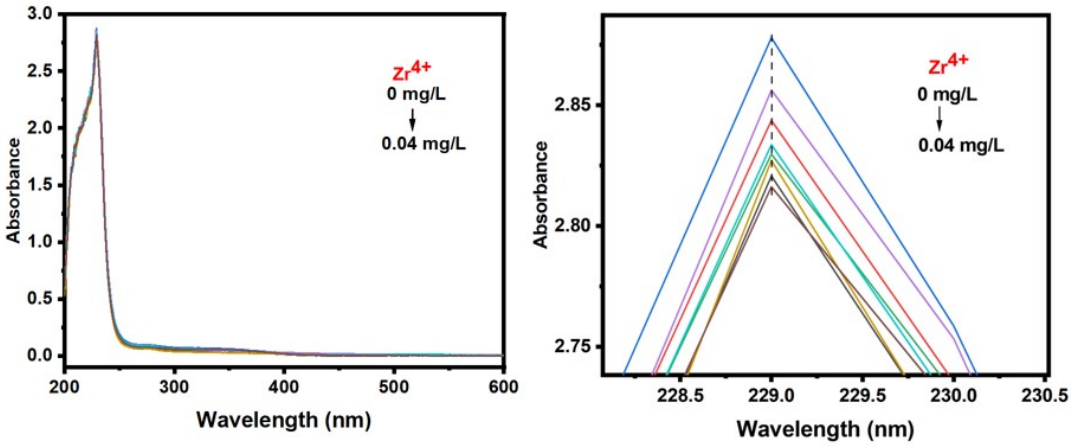

Figure S32. UV/vis absorption of **NAIE-Zr** in $CHCl_3/CH_3OH$ (v/v, 1:3) with different concentrations at 298 K.

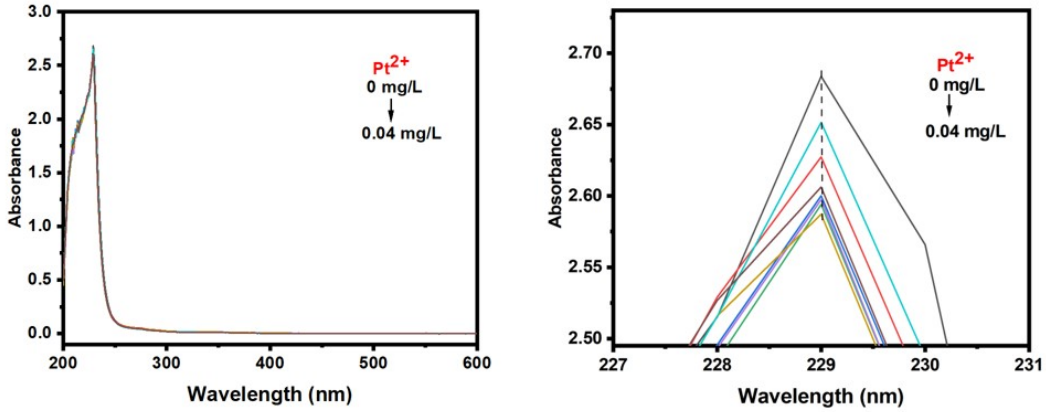

Figure S33. UV/vis absorption of **NAIE-Pt** in $CHCl_3/CH_3OH$ (v/v, 1:3) with different concentrations

at 298 K.

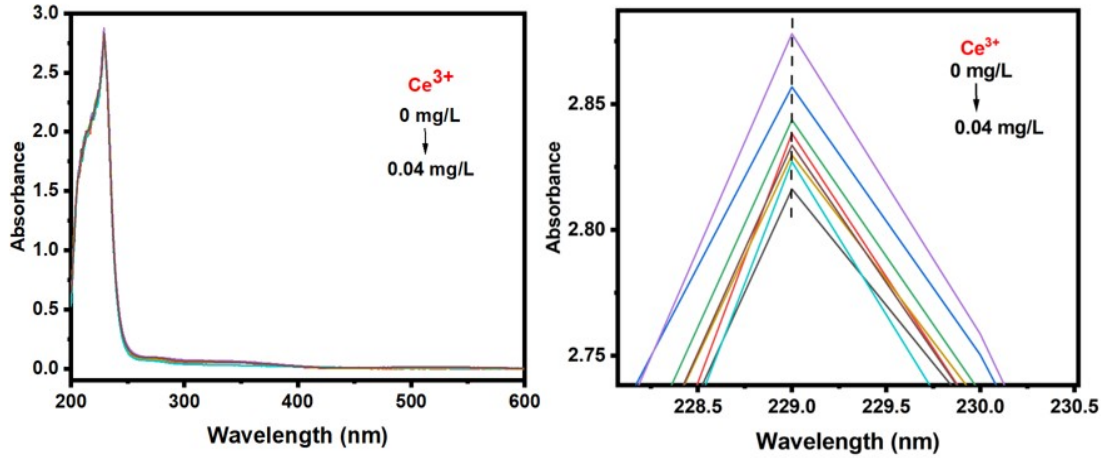

Figure S34. UV/vis absorption of **NAIE-Ce** in $CHCl_3/CH_3OH$ (v/v, 1:3) with different concentrations at 298 K.

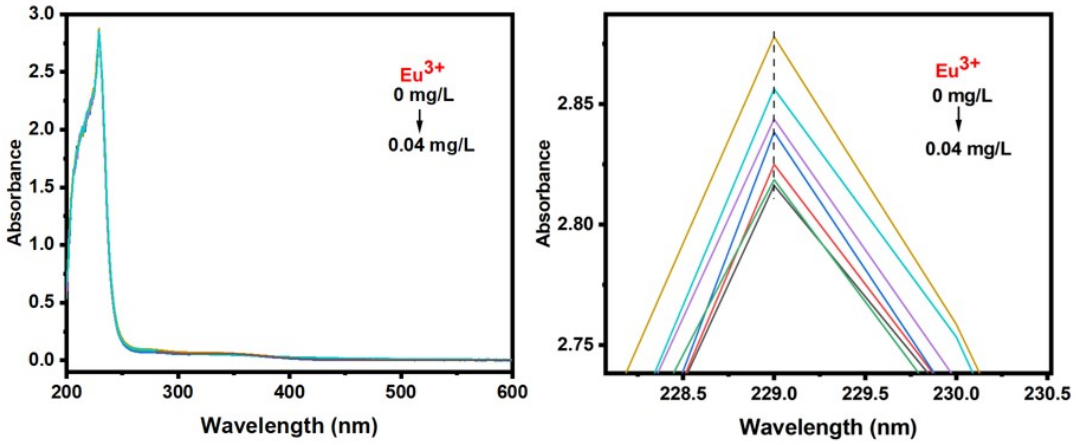

Figure S35. UV/vis absorption of **NAIE-Eu** in $CHCl_3/CH_3OH$ (v/v, 1:3) with different concentrations at 298 K.

Figure S36. Photographs of **L**, **NAIE** in $CHCl_3/CH_3OH$ (v/v, 1:3) (1×10^{-7} M).

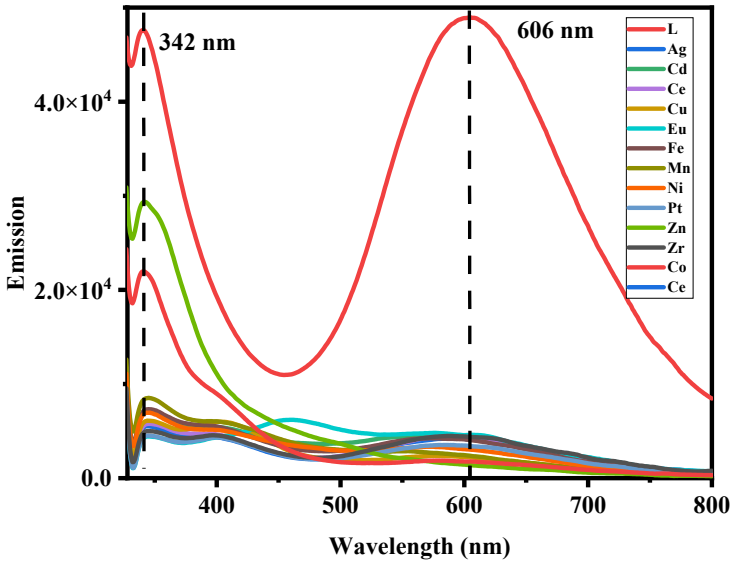

Figure S37. Emission spectrum (1×10^{-7} M in MeOH, 298K, λ_{ex} =285 nm) of **L, NAIE**.

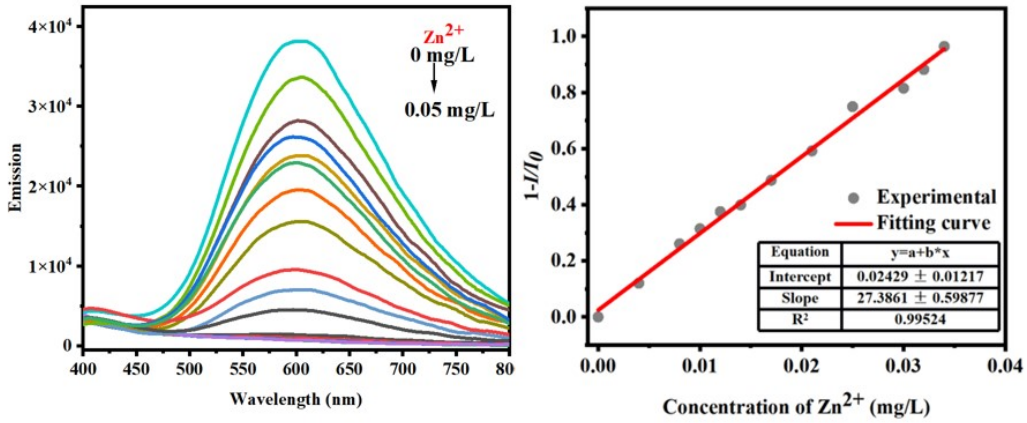

Figure S38. Fluorescence emission spectra of **NAIE-Zn** (1×10^{-7} M in MeOH, 298K) excited at 285 nm after gradual of **Zn^{2+}** (0-0.05 mg/L);The corresponding liner relationship between $1-I/I_0$ and Zn^{2+} concentration of L (I_0 = initial emission intensity of L solution, I = emission intensity after adding different concentrations of Zn^{2+}, C = concentration of Zn^{2+}). The emission intensity of **L** showed a linear correlation with R^2 = 0.99524 with a slope (k) of 27.3861 over the concentration range of (0-0.04 mg/L). The standard deviation (σ) of eight black experiments as 0.01454. The LOD of **L** for Mental against zinc ion in methyl alcohol solution was calculated to be 0.0016 mg/L using the formula LOD= 3σ/k.

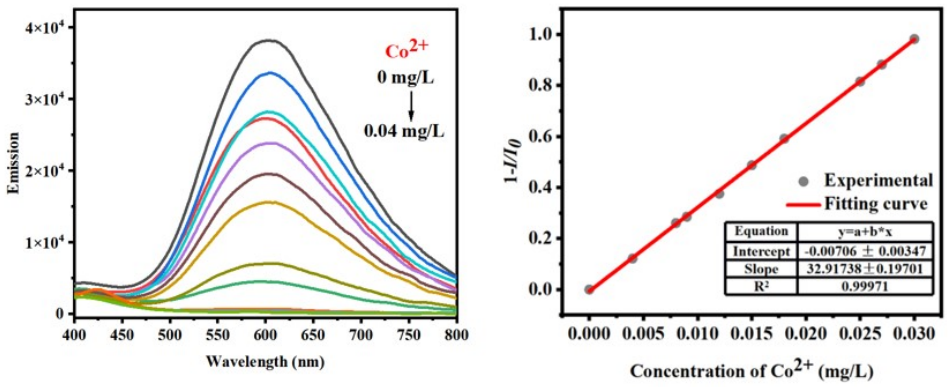

Figure S39. Fluorescence emission spectra of **NAIE-Co** (1×10^{-7} M in MeOH, 298 K) excited at 285 nm after gradually addition of Co^{2+} (0-0.04 mg/L). The detection limit of **L** for Co^{2+} in MeOH solution was calculated to be 0.0013 mg/L.

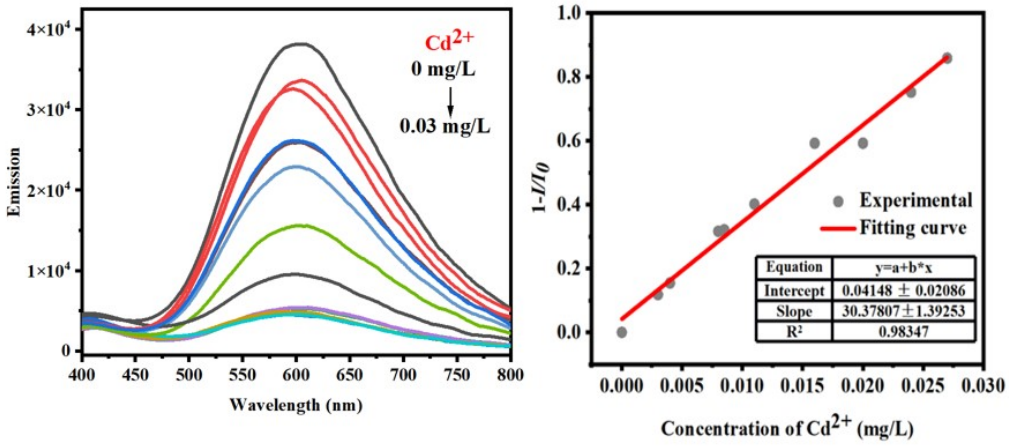

Figure S40. Fluorescence emission spectra of **NAIE-Cd** (1×10^{-7} M in MeOH, 298 K) excited at 285 nm after gradually addition of Cd^{2+} (0-0.03 mg/L). The detection limit of L for Cd^{2+} in MeOH solution was calculated to be 0.00144 mg/L.

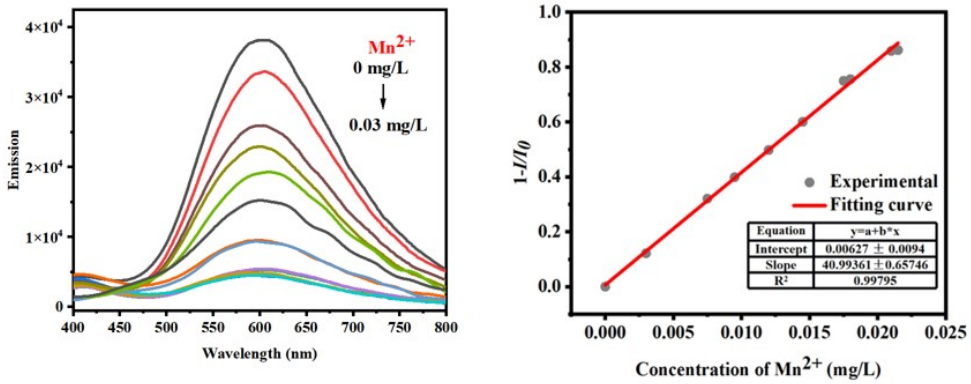

Figure S41. Fluorescence emission spectra of **NAIE-Mn** (1×10^{-7} M in MeOH, 298K) excited at 285 nm after gradually addition of Mn^{2+} (0-0.03 mg/L). The detection limit of **L** for Mn^{2+} in MeOH solution was calculated to be 0.00106 mg/L.

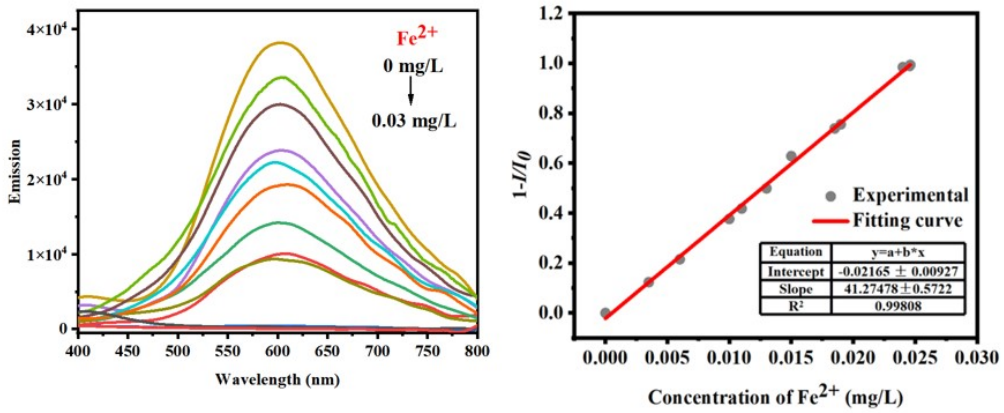

Figure S42. Fluorescence emission spectra of **NAIE-Fe** (1×10^{-7} M in MeOH, 298 K) excited at 285 nm after gradually addition of Fe^{2+} (0-0.03 mg/L). The detection limit of L for Fe^{2+} in MeOH solution was calculated to be 0.001057 mg/L.

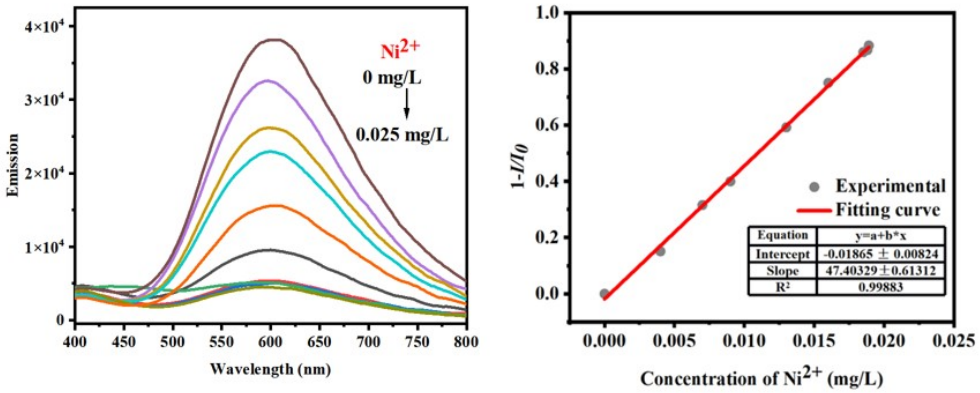

Figure S43. Fluorescence emission spectra of **NAIE-Ni** (1×10^{-7} M in MeOH, 298 K) excited at 285 nm after gradually addition of Ni^{2+} (0-0.025 mg/L). The detection limit of L for Ni^{2+} in MeOH solution was calculated to be 0.00092 mg/L.

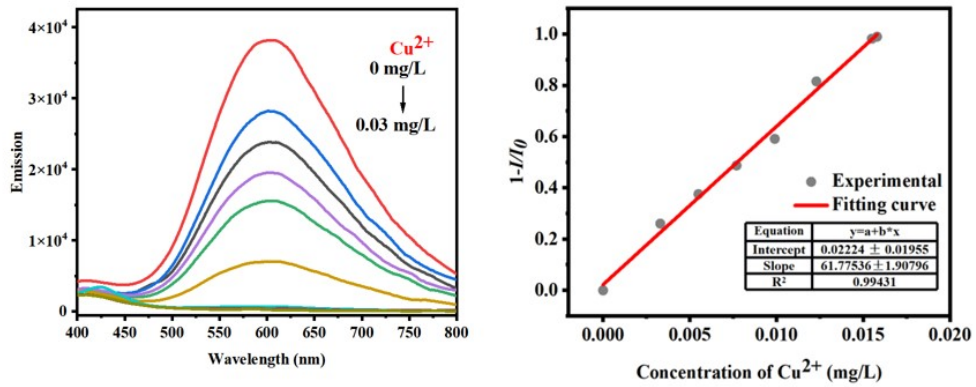

Figure S44. Fluorescence emission spectra of **NAIE-Cu** (1×10^{-7} M in MeOH, 298 K) excited at 285 nm after gradually addition of Cu^{2+} (0-0.03 mg/L). The detection limit of **L** for Cu^{2+} in MeOH solution was calculated to be 0.000706 mg/L.

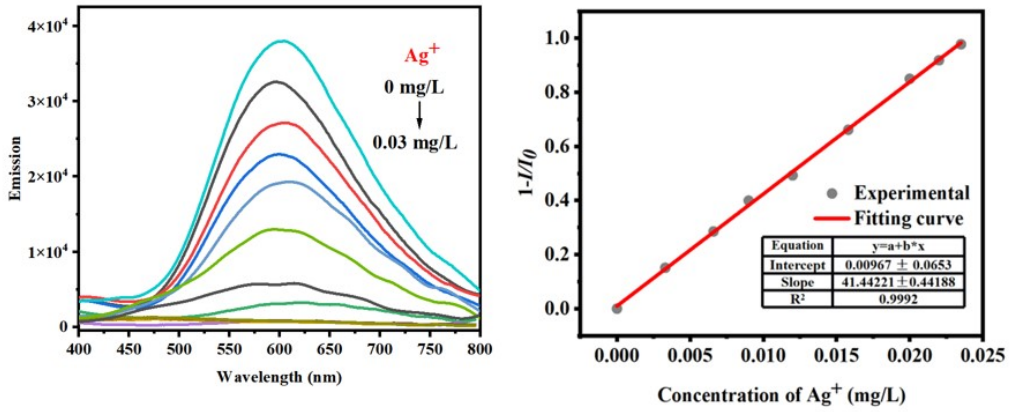

Figure S45. Fluorescence emission spectra of **NAIE-Ag** (1×10^{-7} M in MeOH, 298 K) excited at 285 nm after gradually addition of Ag^{+} (0-0.03 mg/L). The detection limit of **L** for Ag^{+} in MeOH solution was calculated to be 0.001052 mg/L.

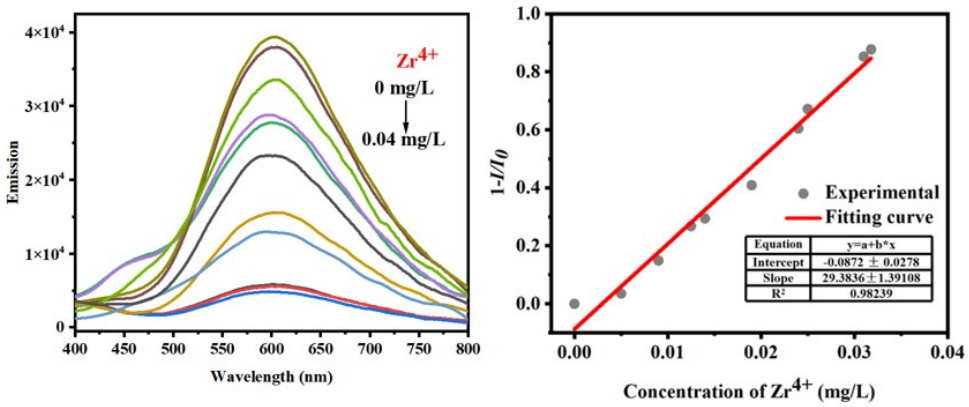

Figure S46. Fluorescence emission spectra of **NAIE-Zr** (1×10^{-7} M in MeOH, 298 K) excited at 285 nm after gradually addition of Zr^{4+} (0-0.04 mg/L). The detection limit of **L** for Zr^{4+} in MeOH solution was calculated to be 0.001485 mg/L.

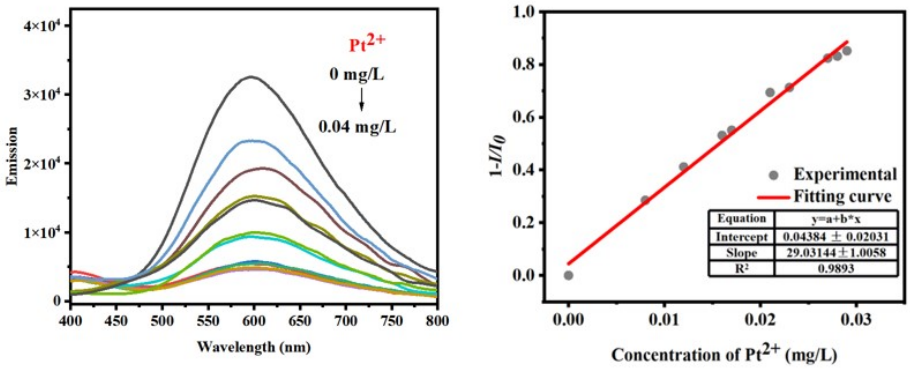

Figure S47. Fluorescence emission spectra of **NAIE-Pt** (1×10^{-7} M in MeOH, 298 K) excited at 285 nm after gradually addition of Pt^{2+} (0-0.04 mg/L). The detection limit of **L** for Pt^{2+} in MeOH solution was calculated to be 0.0015 mg/L.

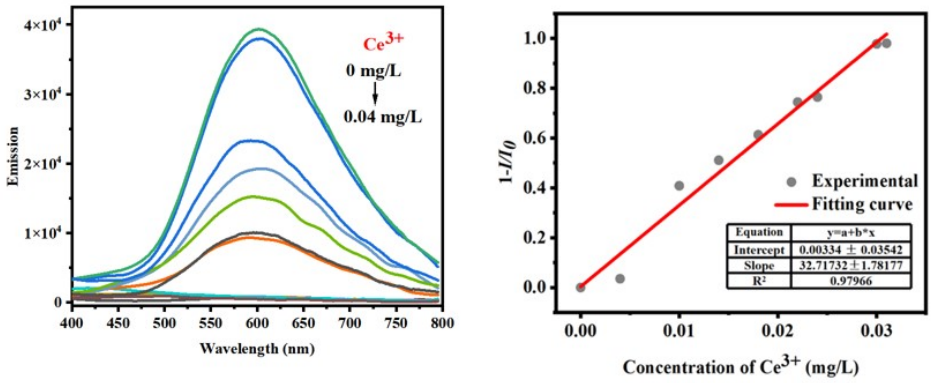

Figure S48. Fluorescence emission spectra of **NAIE-Ce** (1×10^{-7} M in MeOH, 298 K) excited at 285 nm after gradually addition of Ce^{3+} (0-0.04 mg/L). The detection limit of **L** for Ce^{3+} in MeOH solution was calculated to be 0.001333 mg/L.

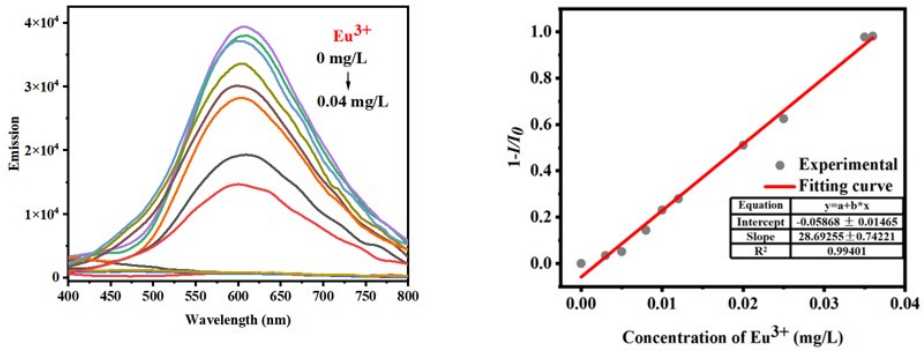

Figure S49. Fluorescence emission spectra of **NAIE-Eu** (1×10^{-7} M in MeOH, 298 K) excited at 285 nm after gradually addition of Eu^{3+} (0-0.04 mg/L). The detection limit of L for Eu^{3+} in MeOH solution was calculated to be 0.00152 mg/L.

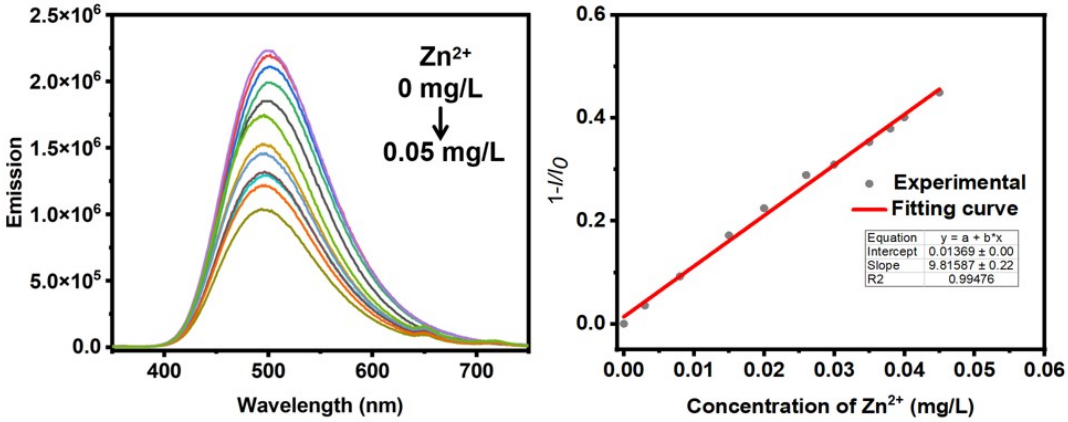

Figure S50. Fluorescence emission spectra of **NAIE-Zn** (1×10^{-7} M in H_2O/DMF (v/v, 40:1), 298K) excited at 295 nm after gradual of **Zn^{2+}** (0-0.05 mg/L);The corresponding liner relationship between 1-*I*/I_0 and Zn^{2+} concentration of L (I_0 = initial emission intensity of L solution, I = emission intensity after adding different concentrations of Zn^{2+}, C = concentration of Zn^{2+}). The emission intensity of **L** showed a linear correlation with R^2 = 0.99476 with a slope (k) of 9.815871 over the concentration

range of (0-0.05 mg/L). The standard deviation (σ) of eight black experiments as 0.0459. The LOD of **L** for Mental against zinc ion in H_2O solution was calculated to be 0.0140 mg/L using the formula LOD= 3σ/k.

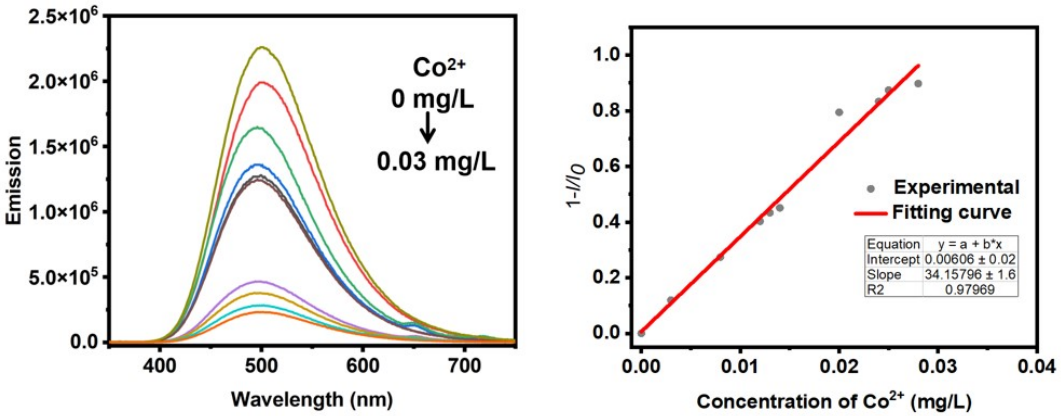

Figure S51. Fluorescence emission spectra of **NAIE-Co** (1×10^{-7} M in H_2O/DMF (v/v, 40:1), 298 K) excited at 295 nm after gradually addition of Co^{2+} (0-0.03 mg/L). The detection limit of **L** for Co^{2+} in H_2O solution was calculated to be 0.0040 mg/L.

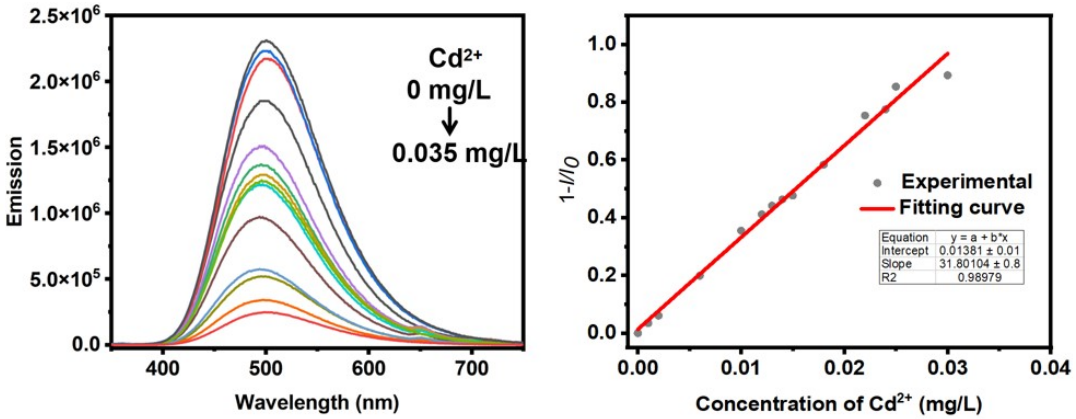

Figure S52. Fluorescence emission spectra of **NAIE-Cd** (1×10^{-7} M in H_2O/DMF (v/v, 40:1), 298 K) excited at 295 nm after gradually addition of Cd^{2+} (0-0.035 mg/L). The detection limit of L for Cd^{2+} in H_2O solution was calculated to be 0.0043 mg/L.

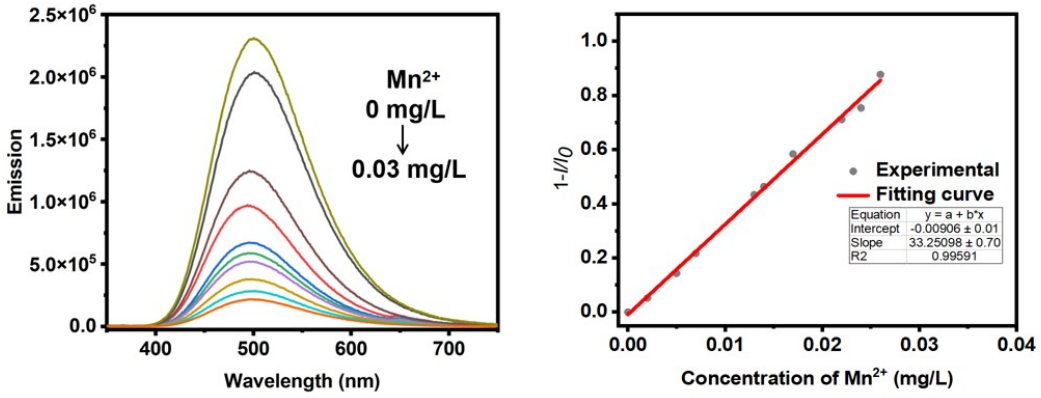

Figure S53. Fluorescence emission spectra of **NAIE-Mn** (1×10^{-7} M in H_2O/DMF (v/v, 40:1), 298K) excited at 295 nm after gradually addition of Mn^{2+} (0-0.03 mg/L). The detection limit of **L** for Mn^{2+} in H_2O solution was calculated to be 0.0041 mg/L.

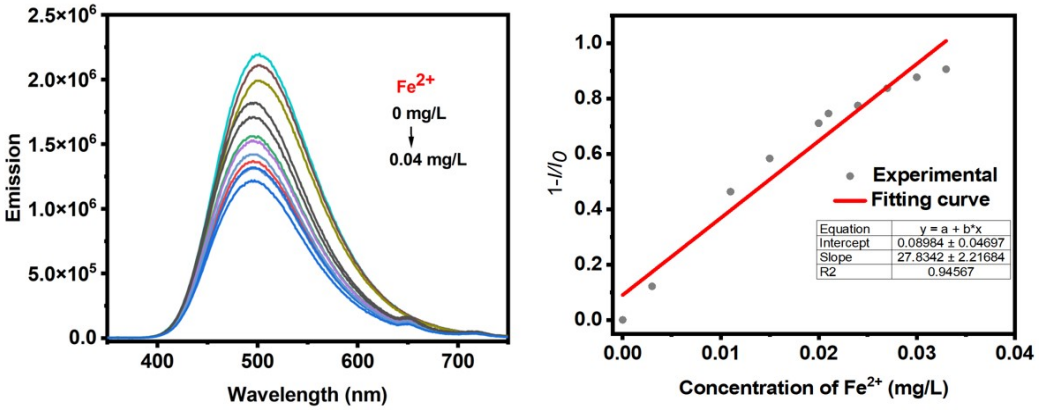

Figure S54. Fluorescence emission spectra of **NAIE-Fe** (1×10^{-7} M in H_2O/DMF (v/v, 40:1), 298 K) excited at 295 nm after gradually addition of Fe^{2+} (0-0.04 mg/L). The detection limit of L for Fe^{2+} in H_2O solution was calculated to be 0.0049 mg/L.

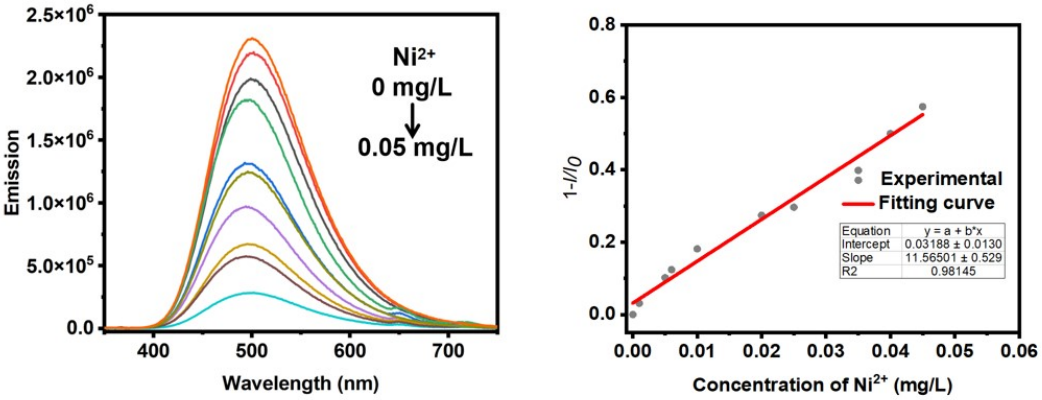

Figure S55. Fluorescence emission spectra of **NAIE-Ni** (1×10^{-7} M in H_2O/DMF (v/v, 40:1), 298 K) excited at 295 nm after gradually addition of Ni^{2+} (0-0.05 mg/L). The detection limit of L for Ni^{2+} in H_2O solution was calculated to be 0.0119 mg/L.

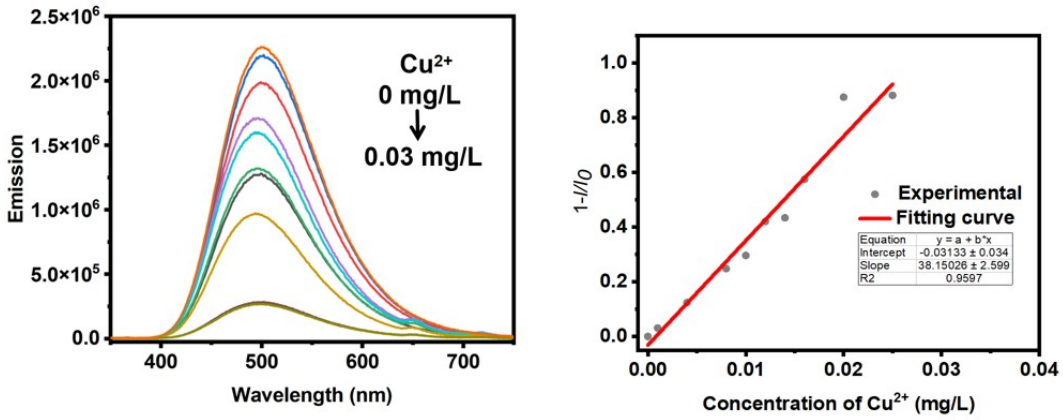

Figure S56. Fluorescence emission spectra of **NAIE-Cu** (1×10^{-7} M in H_2O/DMF (v/v, 40:1), 298 K) excited at 295 nm after gradually addition of Cu^{2+} (0-0.03 mg/L). The detection limit of **L** for Cu^{2+} in H_2O solution was calculated to be 0.0036 mg/L.

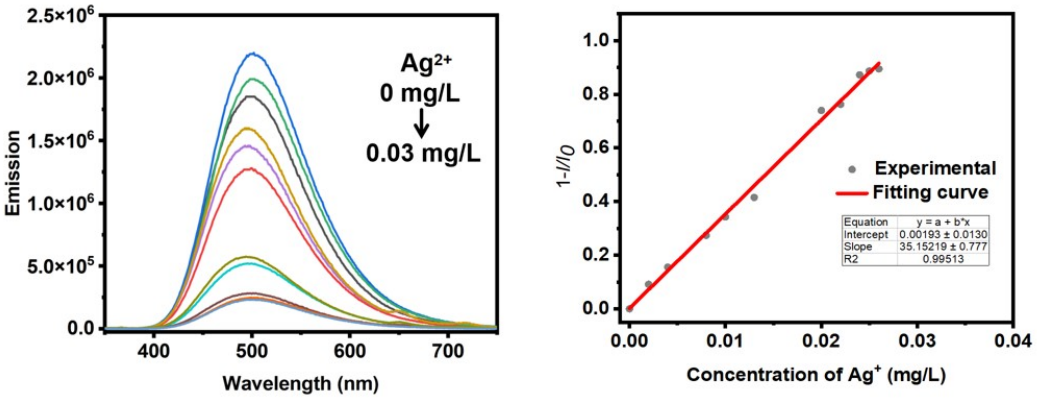

Figure S57. Fluorescence emission spectra of **NAIE-Ag** (1×10^{-7} M in H_2O/DMF (v/v, 40:1), 298 K) excited at 295 nm after gradually addition of Ag^{+} (0-0.03 mg/L). The detection limit of **L** for Ag^{+} in H_2O solution was calculated to be 0.0039 mg/L.

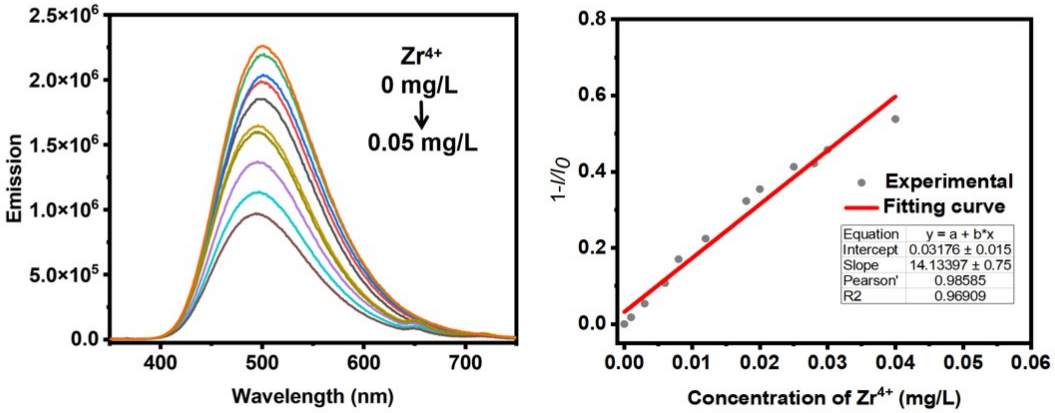

Figure S58. Fluorescence emission spectra of **NAIE-Zr** (1×10^{-7} M in H_2O/DMF (v/v, 40:1), 298 K) excited at 295 nm after gradually addition of Zr^{4+} (0-0.05 mg/L). The detection limit of **L** for Zr^{4+} in

H_2O solution was calculated to be 0.0097 mg/L.

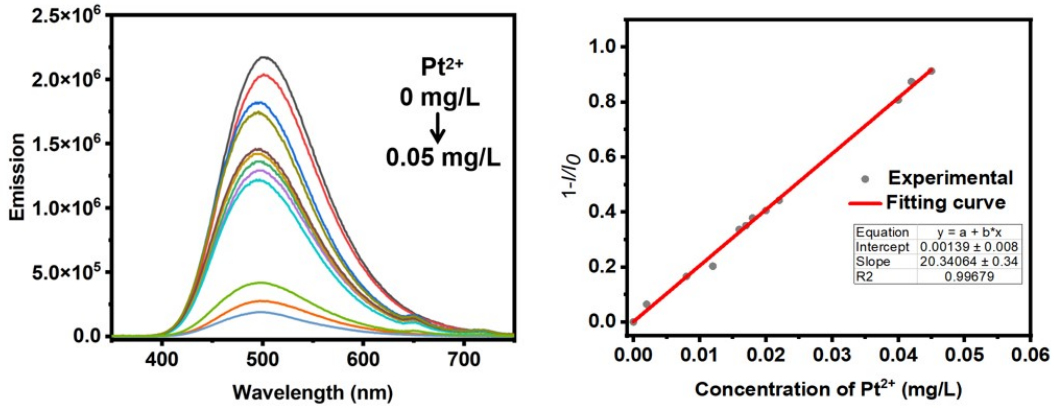

Figure S59. Fluorescence emission spectra of **NAIE-Pt** (1×10^{-7} M in H_2O/DMF (v/v, 40:1), 298 K) excited at 295 nm after gradually addition of Pt^{2+} (0-0.05 mg/L). The detection limit of **L** for Pt^{2+} in H_2O solution was calculated to be 0.0068 mg/L.

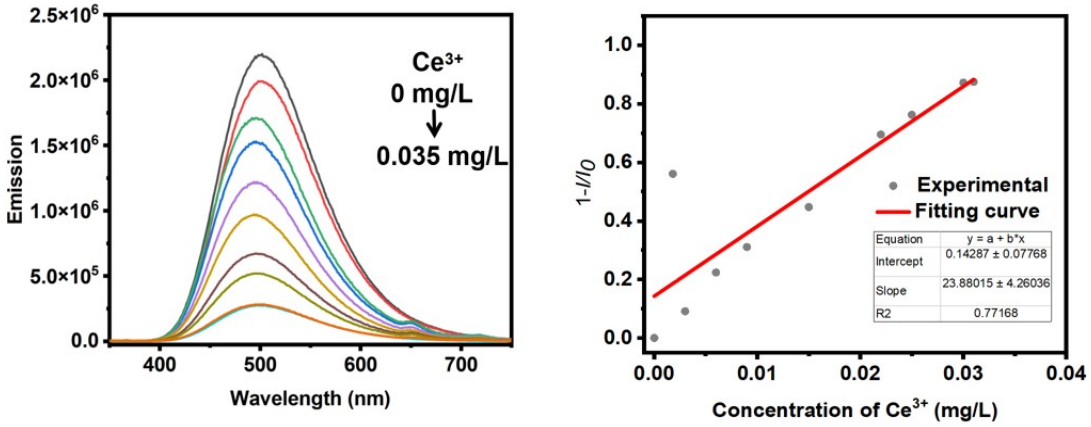

Figure S60. Fluorescence emission spectra of **NAIE-Ce** (1×10^{-7} M in H_2O/DMF (v/v, 40:1), 298 K) excited at 295 nm after gradually addition of Ce^{3+} (0-0.035 mg/L). The detection limit of **L** for Ce^{3+} in H_2O solution was calculated to be 0.0058 mg/L.

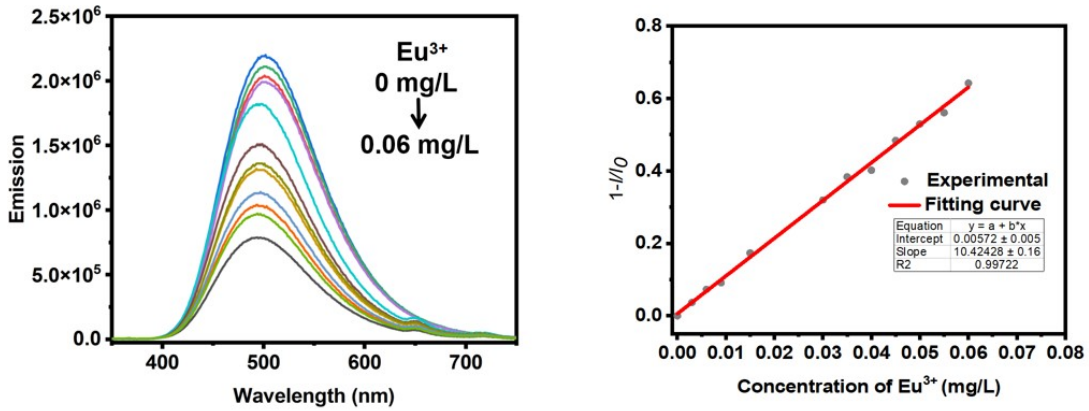

Figure S61. Fluorescence emission spectra of **NAIE-Eu** (1×10^{-7} M in H_2O/DMF (v/v, 40:1), 298 K) excited at 295 nm after gradually addition of Eu^{3+} (0-0.06 mg/L). The detection limit of L for Eu^{3+} in

H_2O solution was calculated to be 0.0132 mg/L.

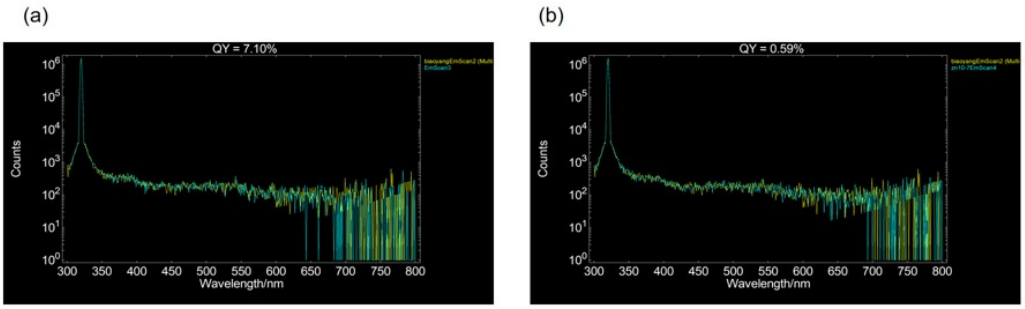

Figure S62. Relative fluorescence quantum yield of **L** and **NAIE** (a: Zn, b: Co) in MeOH at 1×10^{-7} M (298 K).

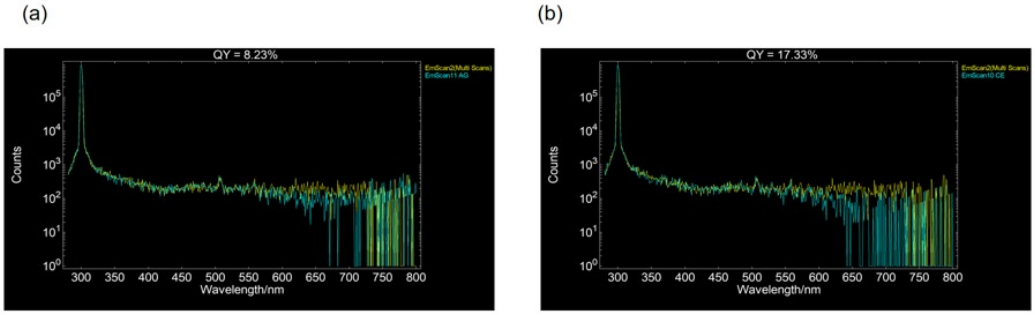

Figure S63. Relative fluorescence quantum yield of **L** and **NAIE** (a: Cu, b: Ce) in MeOH at 1×10^{-7} M (298 K).

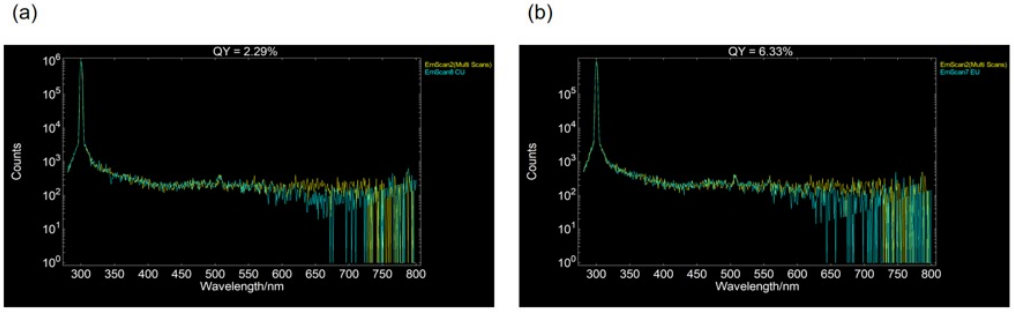

Figure S64. Relative fluorescence quantum yield of **L** and **NAIE** (a: Ag, b: Eu) in MeOH at 1×10^{-7} M (298 K).

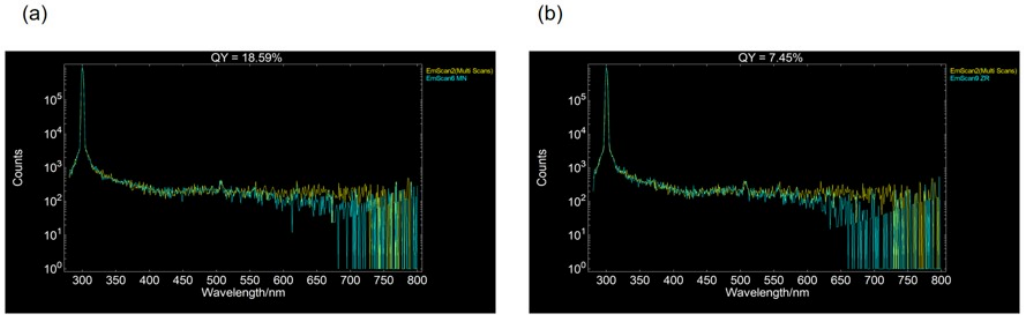

Figure S65. Relative fluorescence quantum yield of **L** and **NAIE** (a: Mn, b: Zr) in MeOH at 1×10^{-7} M (298 K).

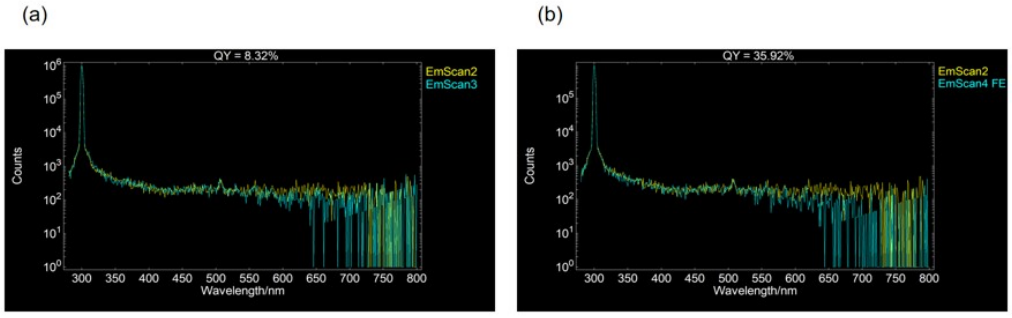

Figure S66. Relative fluorescence quantum yield of **L** and **NAIE** (a: Ni, b: Fe) in MeOH at 1×10^{-7} M (298 K).

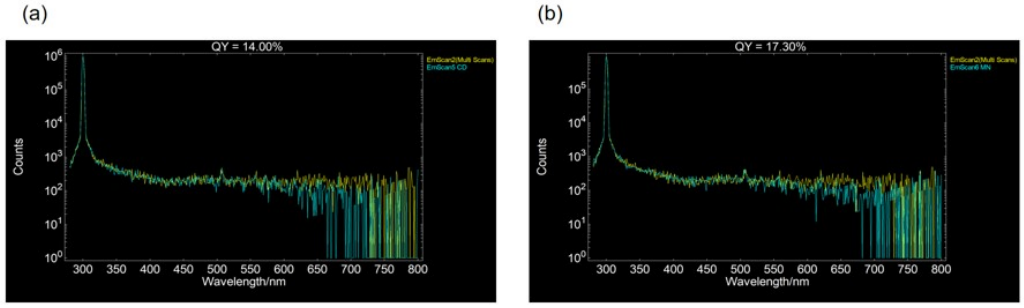

Figure S67. Relative fluorescence quantum yield of **L** and **NAIE** (a: Pt, b: Cd) in MeOH at 1×10^{-7} M (298 K).

9. Fluorescence lifetime plots for L and NAIE

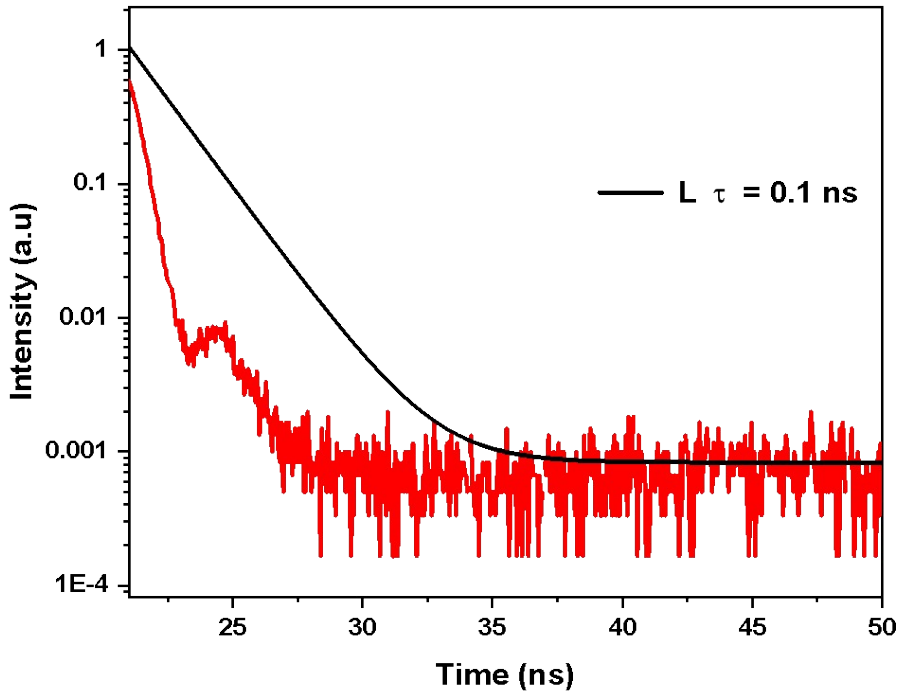

Figure S68. Decay traces of the transient absorption of **L** at 315 nm(1×10^{-7} M in MeOH, 298 K) .

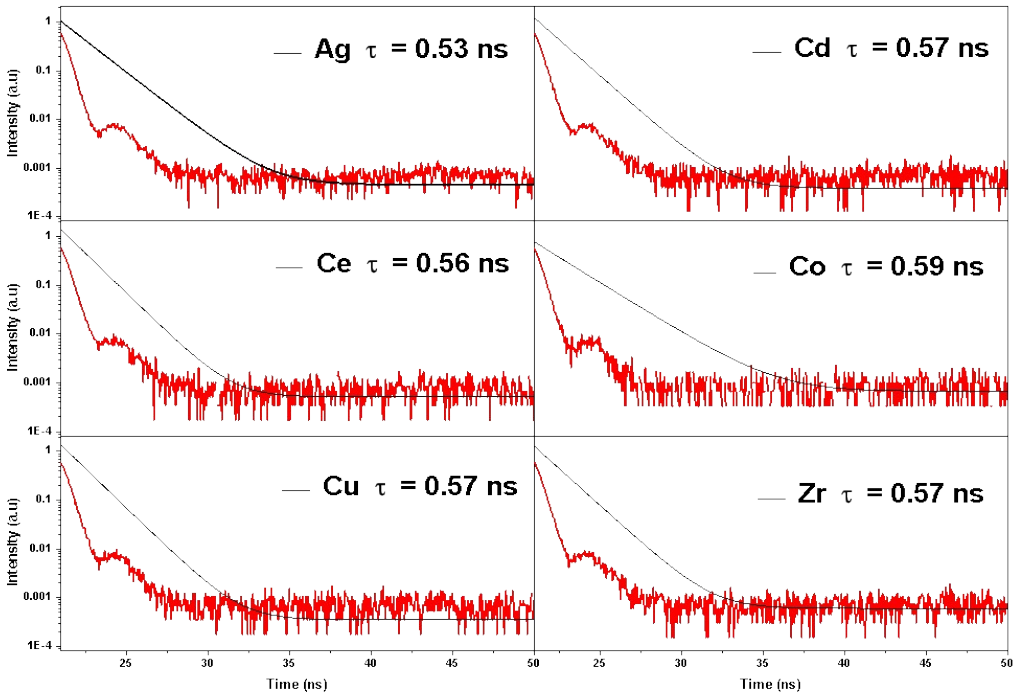

Figure S69. Decay traces of the transient absorption of Ag, Cd, Ce, Co, Cu and Zr at 315 nm(1×10^{-7} M in MeOH, 298 K).

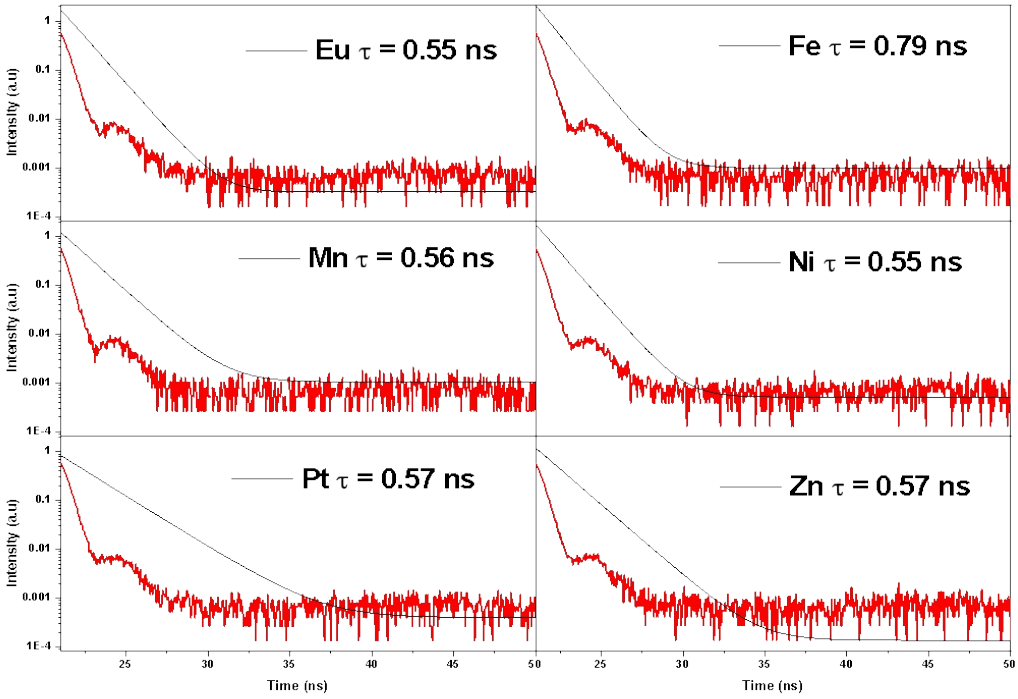

Figure S70. Decay traces of the transient absorption of Eu, Fe, Mn, Ni, Pt and Zn at 315 nm (1×10^{-7} M in MeOH, 298 K).

10. NMR acid-base titration plots of NAIE-Zn

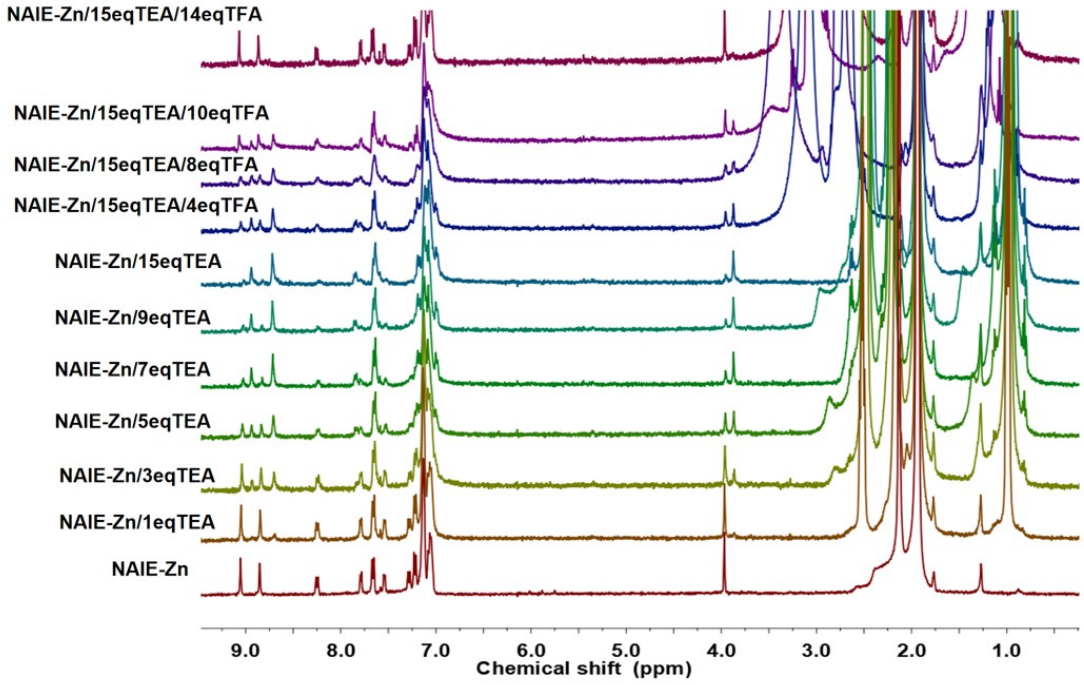

Figure S71. ^{1}H NMR (400 MHz, CD_3CN, 300 K) spectrum acid-base titration of **NAIE-Zn**.

11. Reference

1. M.-Y. Wang, Q.-J. Zhang, Q.-Q. Shen, Q.-Y. Li, S.-J. Ren, *Chin. J. Polym. Sci.* 2020, ***38***, 151-157.

2. H. Tsuji, Y. Ota, S. Furukawa, C. Mitsui, Y. Sato, E. Nakamura, *Asian J. Org. Chem.* 2012, ***1***, 34-37.

3. C. Shang, G. Wang, Y.-C. Wei, Q. Jiang, K. Liu, M. Zhang, Y.-Y. Chen, X. Chang, F. Liu, S. Yin, P.-T. Chou, Y. Fang, *CCS Chem.* 2021, ***4*****,** 1949-1